Multi-Directional Slip Detection Between Artificial Fingers and a Grasped Object

by

Albert Hsia

A Thesis Presented in Partial Fulfillment
of the Requirements for the Degree
Master of Science

Approved April 2012 by the
Graduate Supervisory Committee:

Veronica Santos, Chair
Marco Santello
Stephen Helms Tillery

ARIZONA STATE UNIVERSITY

May 2012

ABSTRACT

Effective tactile sensing in prosthetic and robotic hands is crucial for improving the functionality of such hands and enhancing the user's experience. Thus, improving the range of tactile sensing capabilities is essential for developing versatile artificial hands. Multimodal tactile sensors called BioTacs™, which include a hydrophone and a force electrode array, were used to understand how grip force, contact angle, object texture, and slip direction may be encoded in the sensor data. Findings show that slip induced under conditions of high contact angles and grip forces resulted in significant changes in both AC and DC pressure magnitude and rate of change in pressure. Slip induced under conditions of low contact angles and grip forces resulted in significant changes in the rate of change in electrode impedance. Slip in the distal direction of a precision grip caused significant changes in pressure magnitude and rate of change in pressure, while slip in the radial direction of the wrist caused significant changes in the rate of change in electrode impedance. A strong relationship was established between slip direction and the rate of change in ratios of electrode impedance for radial and ulnar slip relative to the wrist. Consequently, establishing multiple thresholds or establishing a multivariate model may be a useful method for detecting and characterizing slip. Detecting slip for low contact angles could be done by monitoring electrode data, while detecting slip for high contact angles could be done by monitoring pressure data. Predicting slip in the distal direction could be done by monitoring pressure data, while predicting slip in the radial and ulnar directions could be done by monitoring electrode data.

TABLE OF CONTENTS

LIST OF TABLES

LIST OF FIGURES

Chapter 1

DETECTING SLIP DURING SINGLE-DIGIT HAPTIC EXPLORATION

Prosthetic and robotic hand functionality can be greatly enhanced by

improving capabilities for artificial tactile sensing. One of the functions of interest

is the ability for robotic hands to autonomously determine the appropriate

fingertip forces to apply to an object during grasp and manipulation. However,

controlling grip force with a prosthetic or robotic hand requires detailed sensory

feedback information regarding microslips between the artificial fingertips and

the object. In the human hand, this is accomplished with the help of

mechanoreceptors capable of a wide range of functions, such as detecting micro-

vibrations (Figure 1).
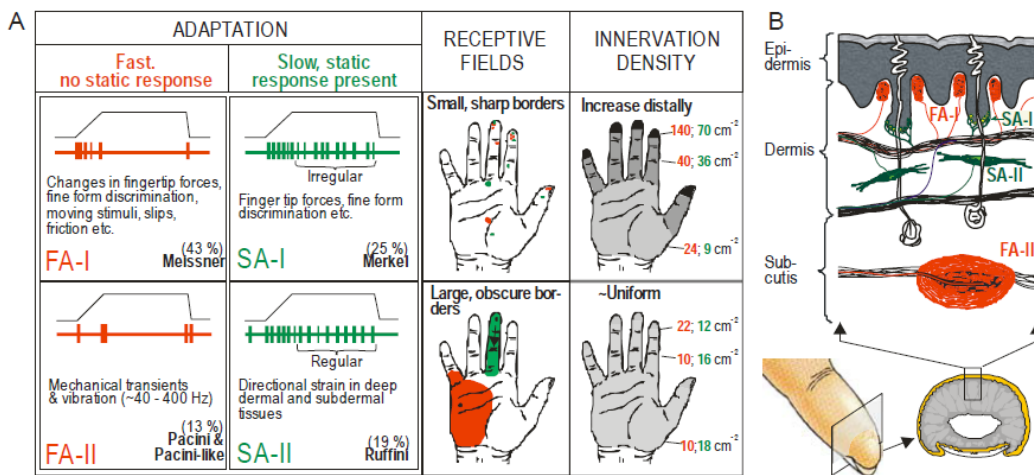
Figure 1. Human Skin Anatomy. (Excerpted from (Johansson & Flanagan, 2008))
Human skin contains a variety of morphologically distinct mechanoreceptors.
This diagram specifically represents the skin of the fingertip. Vibrations are
detected by Pacinian and Meissner corpuscles, which are mechanoreceptors of
interest for slip detection.

There are four main types of mechanoreceptors used for tactile sensing in

the human hand. They are distinguished by the type of stimuli they sense as well

as their location within the layers of the skin. Slow-adapting "SA" afferents sense sustained deformation while fast-adapting "FA" afferents sense dynamic stimuli. Type I afferents are located at the dermal-epidermal margin while type II afferents are located in deeper layers of the skin.

Merkel disk receptors are slow-adapting type I afferents capable of discriminating fine fingertip forces (Johansson & Flanagan, 2008). Ruffini organs are slow-adapting type II afferents capable of detecting directional skin stretch (Purves, 2001). Meissner corpuscles are fast-adapting type I afferents capable of responding to tissue deformations and dynamic mechanical events, such as holding and maneuvering objects (Johansson & Flanagan, 2008). Pacinian corpuscles are fast-adapting type II afferents capable of sensing vibrations from 60 to 500 Hz (Mountcastle, LaMotte, & Carli, 1972). Their ability to detect slight slips provides the hand with a wealth of tactile sensory capabilities (Johansson & Flanagan, 2008).

Emulating these biological mechanotransducers for prosthetic hands can be difficult because of the fragility associated with highly sensitive devices (Fishel, Santos, & Loeb, 2008). A recently developed tactile sensor called the BioTac™ (Syntouch LLC) includes a hydrophone for detecting microvibrations by detecting the rapid changes in pressure caused by slip between the finger and the object, along with an electrode array for detecting changes in applied force at different regions of the finger by measuring the electrodes' impedance as the skin and fluid volume deforms under load (*Figure 2*). BioTac™ sensor components emulate the varied tactile sensing capabitilies of human fingertips. The sensor's

AC pressure data serve as fast-adapting receptors for detecting dynamic stimuli associated with vibrations, slip and textures. The DC pressure and electrode impedance data serve as slow-adapting receptors for detecting sustained loading and deformation of the fingertip that can be related to pressure, force, and skin stretch.
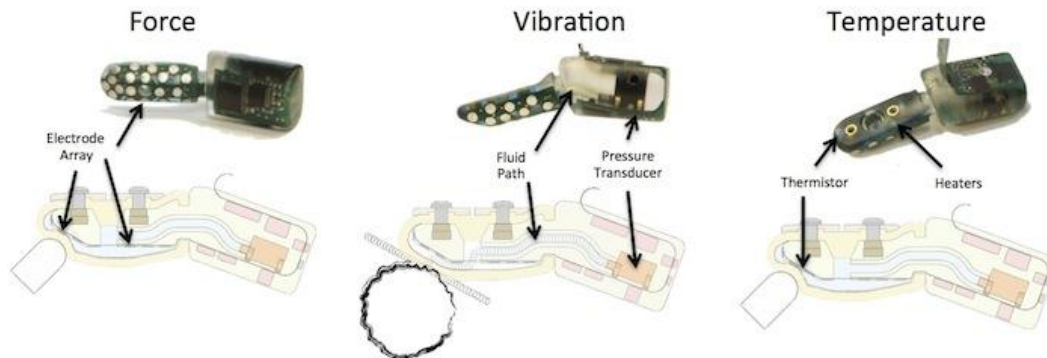
Figure 2. BioTac™ sensor along with mechanical schematic of the sensors' internal components (excerpted from "Syntouch - Technology Overview"). The main components of interest for this first study are the pressure sensor and the electrode array.

The BioTac's electrode arrays have been used to control the grasp of an anthropomorphic prosthetic hand and prevent slip of a grasped cup (N. Wettels, Parnandi, Ji-Hyun Moon, Loeb, & Sukhatme, 2009). The algorithm used fingertip force data (ratio of tangential to normal grip forces) and was designed to sense slip in the ulnar direction of the wrist (N. Wettels et al., 2009). Since slip is not constrained to any one direction, a more robust method of determining the three-dimensional (3D) direction of slip relative to the fingertips is needed.

Additional studies have indicated that the BioTac™ sensor is capable of detecting slip frequencies between 50 Hz to 400 Hz (Fishel et al., 2008). The BioTac™ has been used to determine whether slip occurrences can be detected by

observing fast Fourier transform (FFT) frequency response analyses from the hydrophone's microvibration data. The results showed that slip induced vibrations that were distinctly observable through FFT between 0 Hz and 50 Hz (Hsia, 2011). However, real-time and continuous FFT may drive up the cost of calculation power and time. A simpler and more efficient slip detection method is needed for near real-time control of artificial grasp.

The objective of the present study is to determine how a single BioTac™ sensor's hydrophone and electrode array respond to slip and how features of the finger-object interaction are encoded in the sensor data. Vibration waves caused by slip travel from the finger-object interface, through the skin and fluid, and finally through a channel in the rigid BioTac™ core to the hydrophone. Thus, hydrophone measurements could be affected by the deformable fluid flow path in the artificial fingerpad, which would be affected by fingertip contact area, angle, and force. The following finger-object interaction factors were studied: normal force (0.5N, 1.5N, and 2.5N), finger contact angle (15°, 30°, and 60°), and object texture (150 grit sandpaper and silk). It was hypothesized that multimodal tactile sensor information, from both the sensor's hydrophone and electrode array, could be used to establish an efficient method for detecting specific slip conditions.

MATERIALS AND METHODS

General Experimental Setup. Relative slip between an artificial fingertip and an object can be induced in two different ways: by moving the finger relative to a fixed object, or by moving the object relative to a fixed finger. For simplicity, a motor was used to move a cart relative to a fixed artificial finger. The

4

experimental setup for this experiment was designed to induce slip between an artificial fingertip and an object in contact with varying applied force and contact angle. The contact angle refers to the angle between the object's horizontal surface and the fingernail of the BioTac™ when the two bodies are in contact (Figure 3). The artificial finger was pressed on top of a moving object that was pulled away at a controllable speed and displacement. Data from the artificial finger were collected to understand how each of the three factors affected the sensor's responses, as well as to determine potential methods for detecting slip.
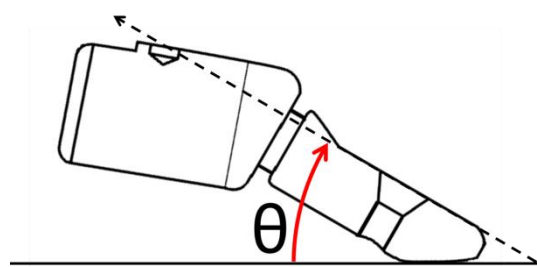
Figure 3. Definition of Contact Angle. Contact angle θ was defined as the angle between the object's surface and the fingernail of the BioTac™ sensor. Only the BioTac™ core is shown here, but the fingernail is parallel to the dorsal surface of the core.

Mounting of Robotic Hand and BioTac™ Sensors. To control the position of the finger throughout the experiment, the BioTac™ sensor was mounted onto a robotic hand called the BarrettHand™ (Barrett Technology, Inc.). An aluminum chassis was constructed for mounting the robotic hand and tactile sensors (Figure 4) for the application of external loads on the artificial fingertips. A middle beam with mounted pulleys was added to allow for a motor to pull the object (a cart with low rolling friction) with a cable at different elevations. Due to the configuration of the robotic hand, the middle digit could be lowered and raised

to control the contact angle between the finger and cart surface. The cart rolled

along a smooth surface which was rigidly attached to two Nano-25 force/torque

transducers (ATI Industrial Automation) for the measurement of the normal force

applied by the artificial fingertip. Clamps were used to secure the chassis to a

rigid lab bench to minimize sensor noise due to movement of the experimental

setup itself.
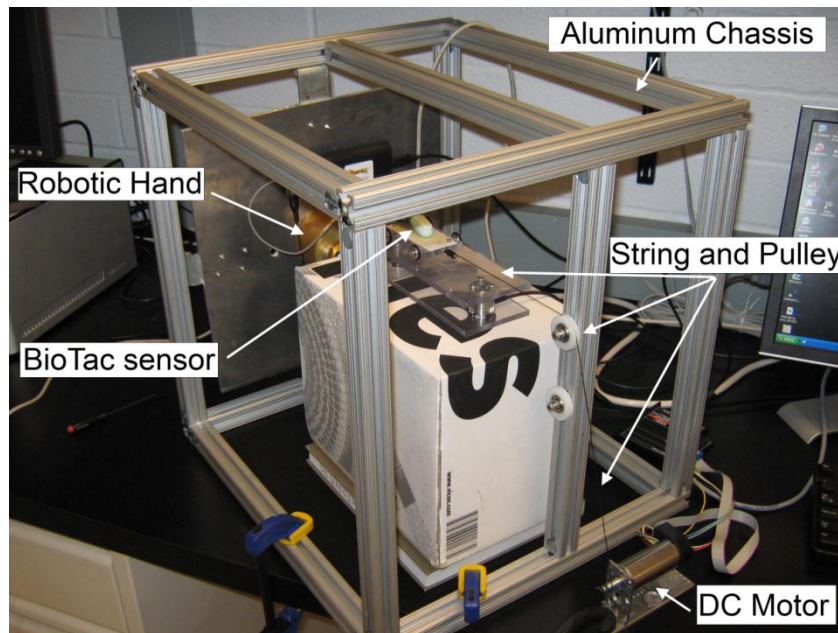
Figure 4. Setup for Slip Detection Experiment. The contact angle of the BioTac
was adjusted by flexing/extending the robotic digit and height of the cart platform
simultaneously.

Load Cell Platform and Texture-Mounted Cart. Once the BioTac™

sensor was attached to the robotic hand, it was lowered onto a texture-mounted

cart that rested on top of a load cell plate. The cart consisted of an acrylic plate

with four rubberized bearings for wheels (Figure 5). Different textures could be

attached to the interchangeable white plates mounted on top of the cart. The front

of the cart consisted of a cable attached to a screw and secured with heat shrink

tubing, which was connected via an inextensible cable to the sheave of a nearby motor that drove the quick sliding pertubations. As the motor winds the cable, the cart moves while the finger is in contact with the texture plate, which resulted in a slip between the artificial finger and textured surface.
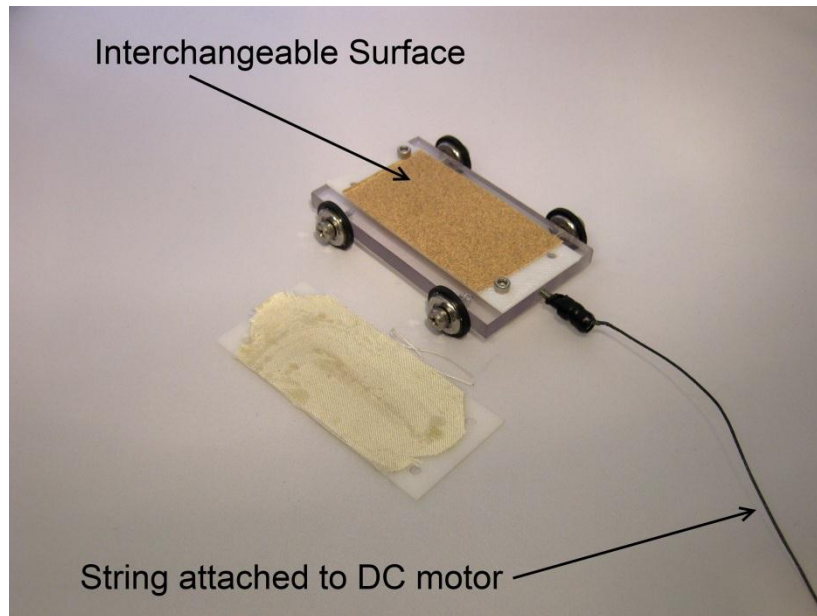
Figure 5. Texture Cart. Different texture can be mounted onto the cart.

The cart rested on top of a load cell platform (Figure 6), which served as the track on which the cart moved during the experiment. The load cell platform was made of two Nano-25 force/torque transducers (ATI Industrial Automation) that were rigidly attached to parallel acrylic plates on its upper and lower surfaces. The platform was used to monitor the applied force of the artificial finger to ensure consistency for each trial in real-time. For experimental consistency, the cart must rest and travel within the boundary of the two transducers. Putting the cart near the tip of the platform may treat the closest transducer as a pivot and induce a moment near the other transducer. The output of the load cells have been

7

known to vary by ±0.5N and often required bias adjustments. As a result, the load cell output needed to be frequently monitored and adjusted throughout the experiment to reduce variability and experimental error.
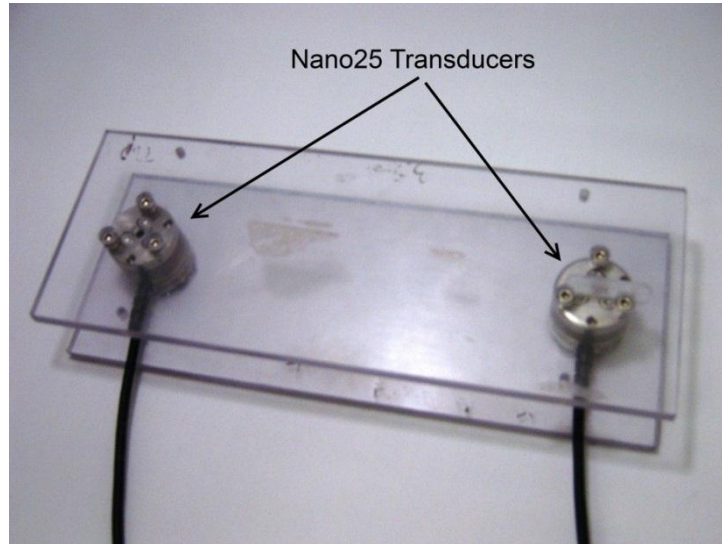
Figure 6. Load Cell Platform. The texture cart was placed on top of the platform. The cart was limited to only moving between the two load cells to reduce the likelihood of creating moments on the edges of the platform.

Slip Induction and Data Acquisition. To simulate slip, a DC motor (EC-max 30, 60 watt, Maxon Motors) rotated at a controlled speed and wound the attached cable and cart until the desired distance had been travelled. Controlling the motor's rotational speed and total displacement was done through a PID controller, which interfaced with the motor control program. As the motor wound the cable, it pulled the cart beneath the stationary artificial fingertip that was in contact with the texture at a specific contact angle (Figure 7). The cable passed through a pulley so that the direction of drag was parallel to the load cell plate and directly away from the BioTac™ sensor. For this experiment, the speed of slip was fixed at 100 mm/s and a displacement of 20 mm. Since the robotic hand

8

moved the BioTac™ sensor into different positions while experimenting with different contact angles, it was also necessary to modify the height at which the load cell plate and texture cart were placed.
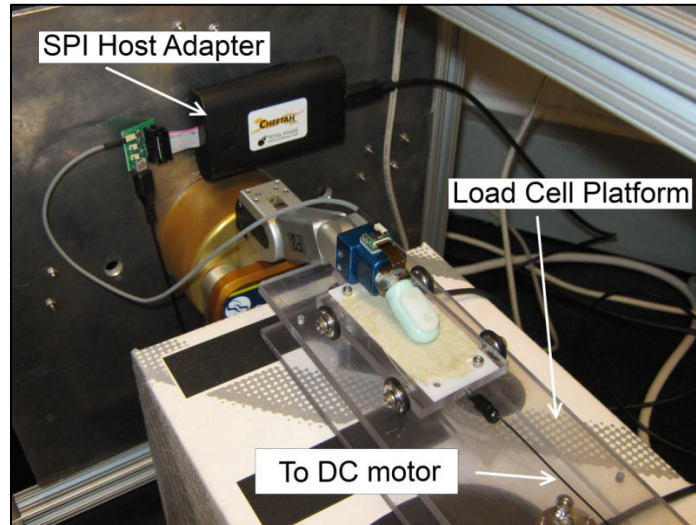
Figure 7. Setup for Data Collection. The texture cart is dragged by the motor, which induces a slip between the finger and the texture. Sensor data travels through the SPI host adapter and then to the computer.

Data acquisition was controlled by a Windows-based C++ program that collected 5 seconds of data after program execution. The motor was controlled by a Linux based C-code program that ran the motor 2 seconds after execution. Data were collected by manually executing both the data acquisition program and the motor program simultaneously from two different computers. 5 seconds of data were collected with slip occurring 2 seconds after program execution. Information from the BioTac™ sensor were then passed through an SPI host adapter (Total Phase, Cheetah SPI Host Adapter) and then to the computer. For this experiment, AC pressure, DC pressure, and electrode impedance data were collected from the BioTac™ sensor. AC pressure had a sampling rate of 2200 Hz, and DC pressure
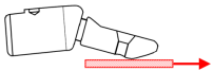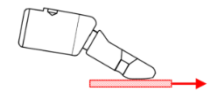
and electrode impedances had a sampling rate of 100 Hz. Baseline trials, where

no slip and no contact with an object occurred, were also collected and used to

preprocess data sets.

Experimental Design. The experiment called for the testing of three

different contact angles, three different applied forces, and two types of textures.

Slip speed and slip length were fixed to reduce the number of factors for this

experiment. Four trials were conducted for each combination of contact angles,

applied forces, and types of textures. A total of 72 trials were conducted.

Table 1 shows the full experimental design of this experiment:

Table 1

Experimental Design for Detecting Slip

Finger Position	Contact Angle	Applied Force	Texture
	15°	0.5 N	150 Grit Sandpaper
	30°	1.5N	Silk
	60°	2.5N	

Slip condition for all trials was fixed at 20 mm at 100mm/s. This value

was chosen because it adequately simulated the speed with which human

fingertips might explore an object (Hsia, 2011). The lowest contact angle that was

achievable with the experimental setup was 15°. Any angle lower resulted in the

robotic hand pushing onto the load cell plate (Figure 8). Angles of 30° and 60°

were chosen because of their similarity to the angle of the fingertip during human

tactile exploration.
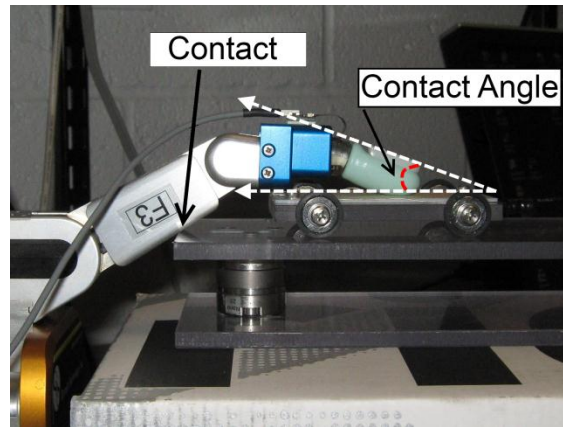
Figure 8. Load Cell Platform Contact. The experimental setup was such that 15°
was the minimum contact angle that could be implemented before the
BarrettHand finger contacted the load cell platform.

Initial test trials indicated that BioTac™ sensors information began to

become noticeable after 0.5 N of applied force. Thus, 0.5 N was established as the

lowest level for applied force, followed by different factor levels at 1.5 N and

2.5N. The experiment called for two textures that were distinctively different.

This was done to check whether slip information from the BioTac™ were similar

for different textures. Consequently, 150 grit sandpaper and silk fabric were

chosen for this experiment. Slip speed and slip length were established based on

initial tests to emulate a human slip during haptic exploration. A slip speed of 100

mm/s with a slip length of 20 mm appeared to be a sufficient model for slip

during haptic exploration.

Data Analysis. The signals of interest from the BioTac™ sensor were AC

pressure, DC pressure, and electrode impedance. Raw voltage data from the

pressure sensor housed in the BioTac™ sensor was converted to engineering units with the following equation:

$$P_{AC} = (x - x_{baseline}) * 5.4211762 * 10^{-5} \ {}^{psi}/_V \tag{1}$$

where *x* was the raw voltage signal and $x_{baseline}$ was the average voltage of a baseline trial. Raw voltage data for DC pressure was converted to engineering units with the following equation:

$$P_{DC} = (x - x_{baseline}) * 5.372 * 10^{-3} \ {}^{psi}/_V \tag{2}$$

where *x* was the raw voltage signal and $x_{baseline}$ is the average voltage of a baseline trial. Raw voltage data for electrode impedance was converted to engineering units and calibrated with the following equation:

$$I_i = \frac{40950 - 10*(x_i - x_{baseline_i})}{(x_i - x_{baseline_i})} \ k\Omega \quad i = 1, 2, \dots 19 \tag{3}$$

where *x* was the raw voltage signal, $x_{baseline}$ was the average voltage of a baseline trial for each of the electrodes, and *i* corresponded to the 19 total electrodes on the BioTac™ sensor. Converted values for the electrode impedance data were referred as impedance change. Skin bulging near an electrode would exhibit a negative impedance change, while depressing the skin near an electrode could exhibit a positive impedance change (Wettels & Loeb, 2011).

Initial tests trials had shown a notable trend in AC pressure data where the pressure rapidly decreased after onset of slip. An assessment on the effect of the various factors on the magnitude of the pressure change was performed, as well as an assessment on the effect of the various factors on the rate of change in pressure

12

after onset of slip. Studies have shown that human hands take about 70 ms to adjust grip forces to compensate for perturbations (Johansson & Flanagan, 2008), while other studies have shown that human grip responses have reacted to slipping objects as early as 60 ms (Cole & Abbs, 1988). The experiments described in this study were focused on assessing how fast the tactile sensors could detect slip and slip direction. No automated grip responses were implemented. A range of pressure drop rates were calculated by using different sampling windows after onset of slip. For example, a sampling window of 10 ms would mean calculating the rate of change in pressure between the onset of slip and 10 ms after slip. Magnitude and rate of change assessment were also performed on DC pressure data. Due to the low sampling rate of DC pressure (100 Hz), calculating the rate of change in pressure was done in 10 ms increments.

The rate of change in impedance was calculated by using different sampling windows. Another assessment was conducted to benchmark different sampling windows by comparing the ratio of rate of change in impedance between two electrodes that were along the same direction of slip. An effective method for graphically representing all 19 electrodes was to display them with respect to their relative position on the finger. Figure 9 shows the layout of the 19 electrodes from a bird's-eye view and plotted on an XY-plane. Electrode 7 was located on the very tip of the finger, whereas electrode 19 resides at the back. Electrode 11 and Electrode 1 are located on the radial and ulnar aspect of the finger, respectively (see Figure 7 for orientation). This XY-plane was used

throughout the analysis on electrode impedance data. Displaying impedance information on a 2D plot could be done by re-ordering plots with respect to their position along the y-axis. Thus, the first point would display information from the tip (Electrode 7), and the last point would display information from the back (Electrode 19). Electrodes on the same y-position would be ordered radial first.
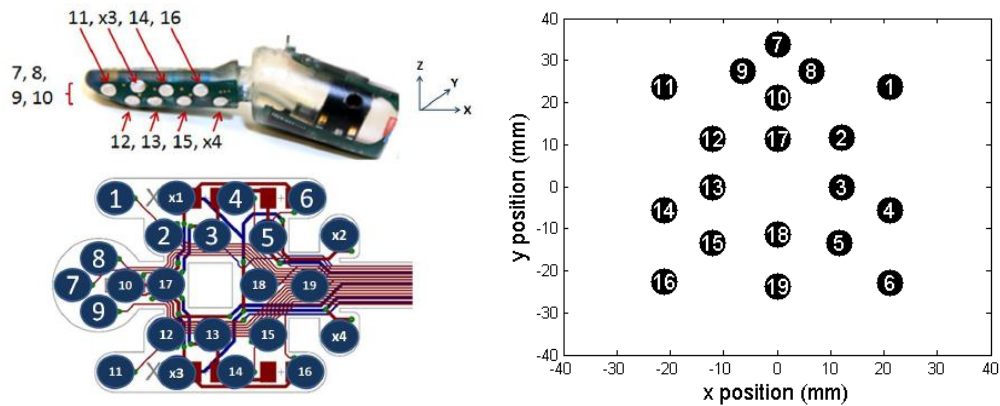
Figure 9. Electrode Array Position. (left image excerpted from (Wettels, 2011) Electrode positions were shown with respect to their distances to other electrodes. The coordinate system established the origin at the opening of the hydrophone.

RESULTS AND DISCUSSION

General Sensor Response. Sensor responses indicated successful data collection for AC pressure, DC pressure, and electrode impedance (Figure 10). Very little noise was observed in the three datastreams. Since variability in all channels of data appeared to be relatively low, collecting four trials for each factor level was considered sufficient to represent the variability of the data.
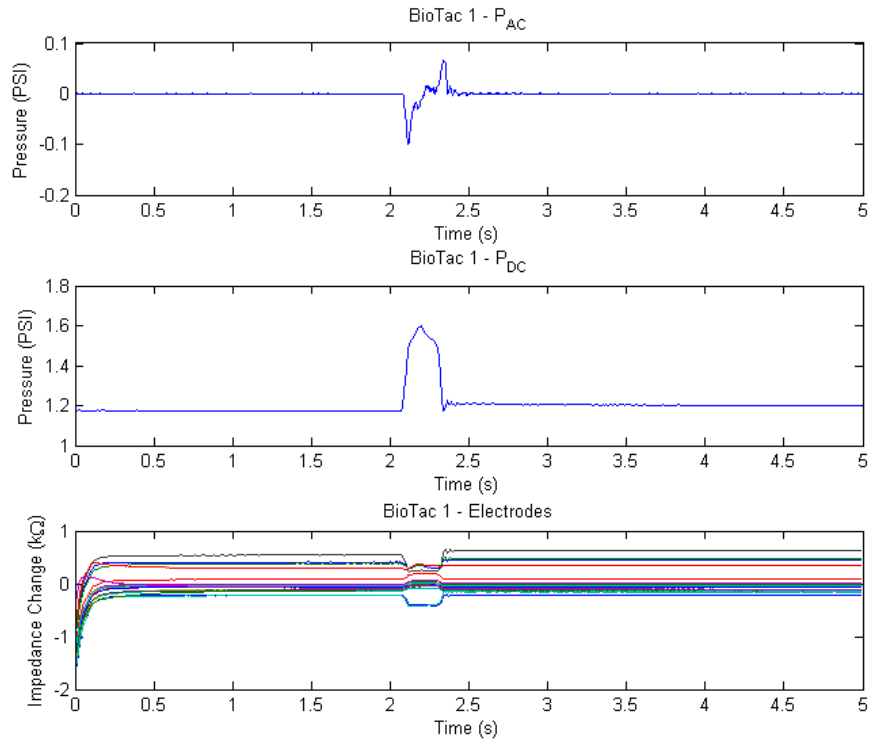
Figure 10. General Appearance of Data. AC pressure, DC pressure, and impedance are collected simultaneously and then analyzed.

AC Pressure Assessment. The first analysis on AC pressure compared the effects of each experimental factor on the magnitude of the pressure drop. The pressure drop appeared to occur immediately after onset of slip. Figure 11 shows the gradual increase in the magnitude of the magnitude of the pressure drop. Contact angles were color-coded to their respective colors. Different textures were labeled with different line styles and marker shapes, and each marker indicates the individual trials' magnitudes. In this figure, the lines represented the average of all 4 trials of their respective group. Magnitude of the AC pressure drop appeared to increase as applied force and contact angle increased for both silk and sandpaper textures. Furthermore, AC pressure magnitude saturated at 0.1 psi.

15
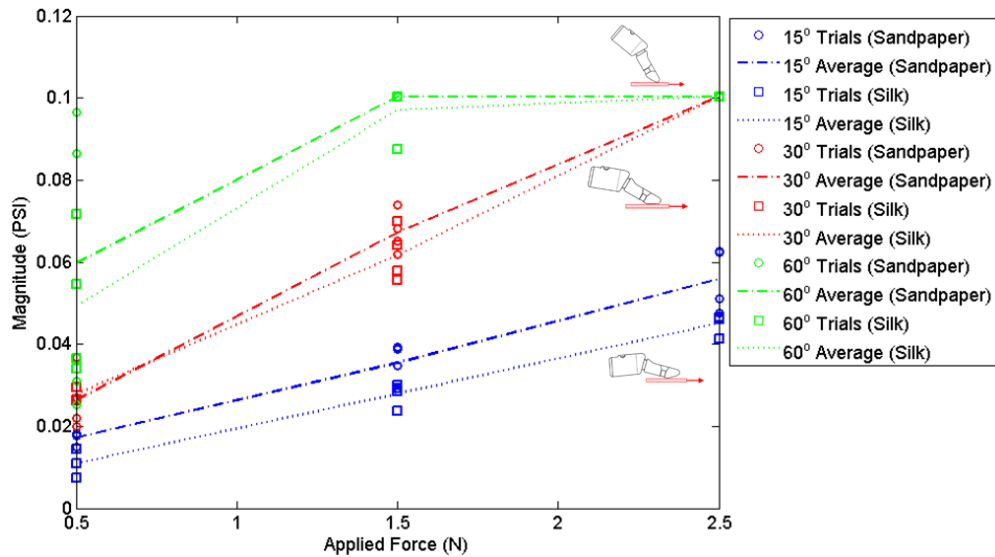
Figure 11. Absolute Magnitude of AC Pressure Drop. Note that high contact angles (60°) still exhibit large magnitude values for low applied forces (0.5N). The absolute values of the drop in AC pressure are shown.

Saturation was observed in other trials as well (Figure 12). Nevertheless, results showed distinct differences in magnitude for different contact angles and applied forces. Thresholding could be an effective method for detecting slip for greater forces and contact angles. For example, if a threshold was established at 0.04 psi, any moment the BioTac™ sensor experiences an AC pressure beyond 0.04 psi would be considered a slip incident. However, AC pressure values from future trials below this threshold would not be detected. In this case, slips occurring in lower contact angles and forces would not be detected. Furthermore, establishing too low of a threshold would increase the chance of detecting false positives. Thus, a threshold could be established that maximizes the chance for slip detection but also reduce the likelihood of detecting false positives.

16
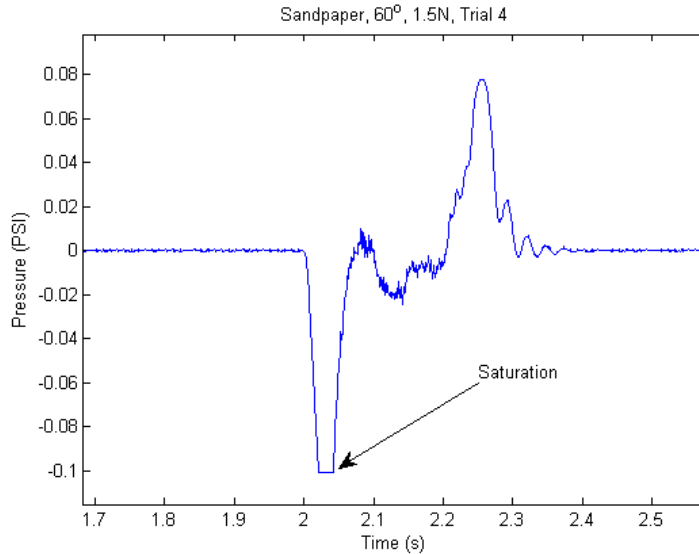
Figure 12. AC Pressure Saturation. -0.1 psi appeared to be the minimum value for AC pressure.

The rate of AC pressure change after onset of slip was also investigated. Different sampling windows were chosen for rate calculation. Figure 13 shows the rate of AC pressure change for different contact angles and applied force. Sampling windows sizes of 3.63 ms (8 sample points), 6.82 ms (15 sample points), 10 ms (22 sample points), 20 ms (44 sample points), and 30 ms (88 sample points) were chosen to observe the effect of different window sizes on rate values. The magnitude of rates appeared to be the greatest at 20 ms. Future analyses on rate of AC pressure changes would use a sampling window of 20 ms.

The rate of AC pressure change appeared to increase in magnitude as contact angles and applied force increased. Since both AC pressure metrics exhibited the same trend. A threshold could be established in either metric that maximized the chance for slip detection but also reduced the likelihood of detecting false positives.

17
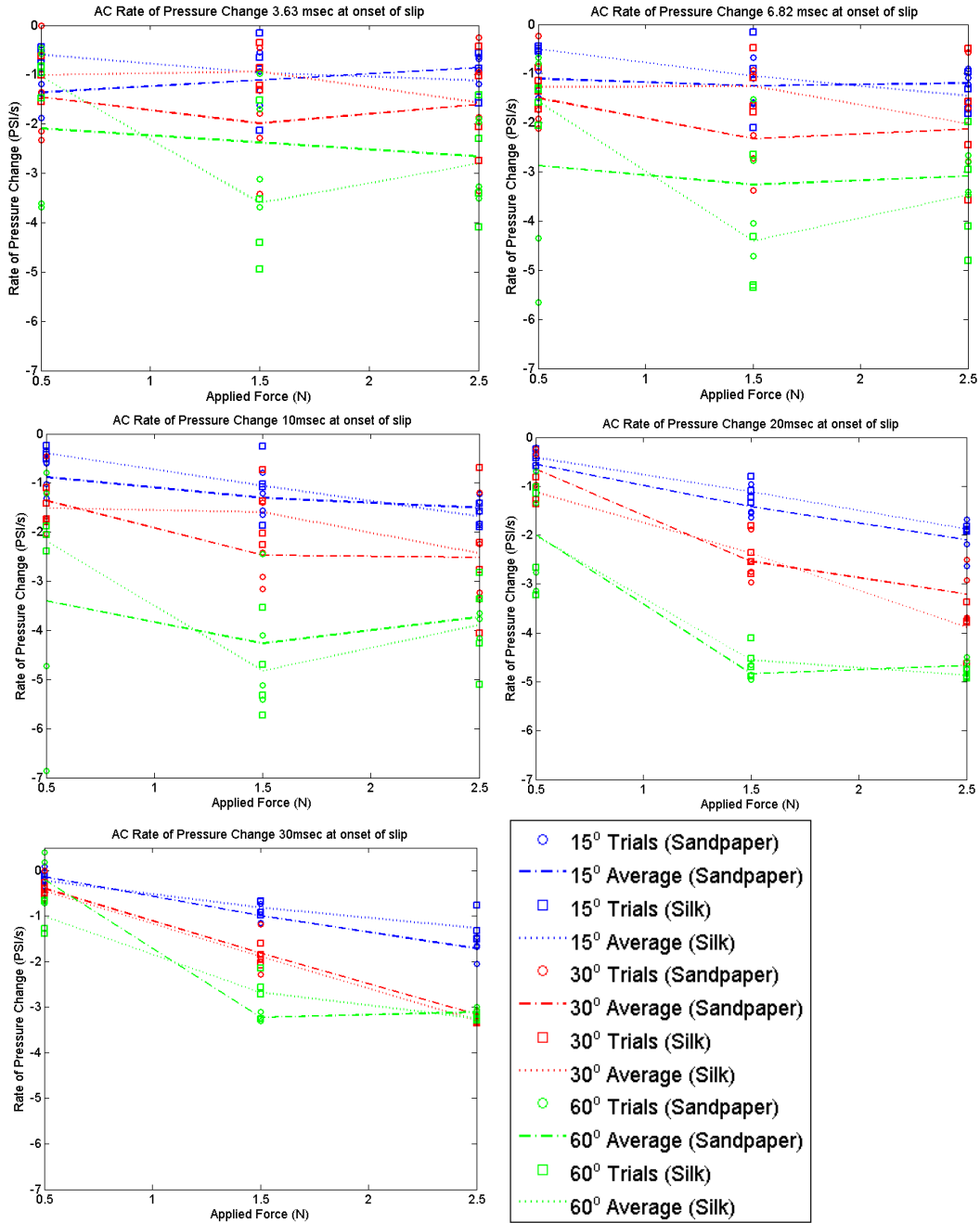
Figure 13. Rate of Change in AC Pressure at Onset of Slip. 20 ms was chosen to be the recommended sampling window because it generated the largest average rate of change in pressure.

DC Pressure Assessment. Analyses conducted on DC pressure data were similar to that of AC pressure. Unlike AC pressure, DC pressure exhibits a rise in

pressure at the onset of slip and does not saturate. Magnitude is calculated by the difference between the maximum DC pressure value during slip and the baseline value before slip. Figure 14 shows the DC magnitude compared to all factors of interest. Similar trends are also exhibited with DC pressure: the magnitude increases as both applied force and contact angle increases. Although sandpaper resulted in a greater DC magnitude than that of silk, both textures exhibited the same trend, in which DC magnitude increased when both contact angle and applied force increased.
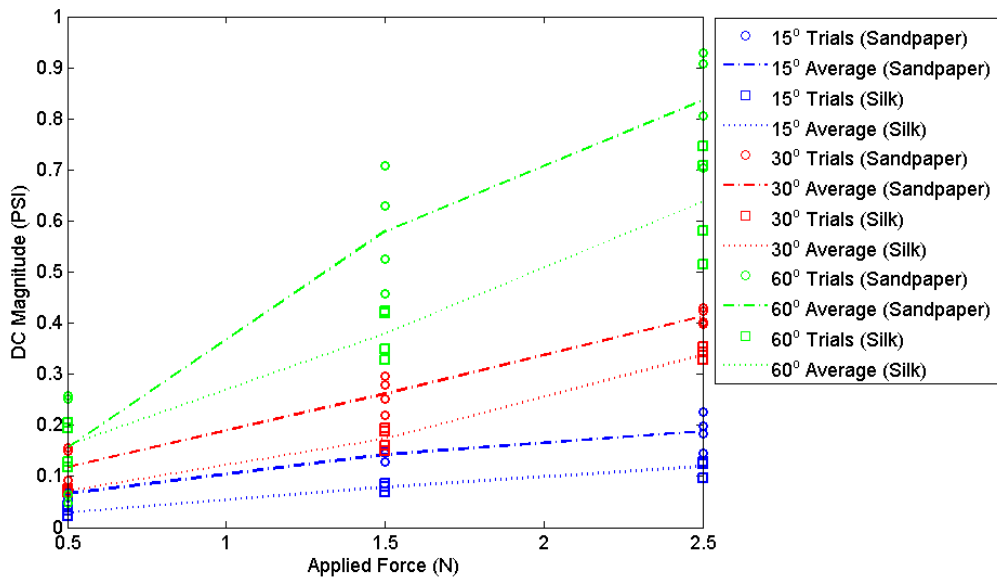
Figure 14. DC Pressure Magnitude. Magnitude increased as both contact angle and applied force increase for both sandpaper and silk texture.

The rate of DC pressure change was also determined with sampling windows of 10 ms (1 sample point), 20 ms (2 sample points), and 30 ms (3 sample points). Figure 15 shows the rate of DC pressure change for all three sampling windows. A sampling window of 30 ms had the largest rate of DC pressure change. Similar to the trends noticed in AC pressure assessment, DC magnitude and rate of DC

19

pressure change both increase as contact angle and applied force increases. Consequently, detecting slip with either DC pressure magnitude or rate of change in pressure would exhibit the same issues found in detecting slip with AC pressure: Lower forces and contact angles require a much more sensitive threshold, which may increase the likelihood of prediction errors caused by non-slip related perturbations. Another drawback would be that the optimal sampling window for DC pressure was 10 ms longer than that of rate of change in AC pressure. Ultimately, applying a threshold in either DC or AC pressure data would not be able to encompass all levels of contact angle and applied force.
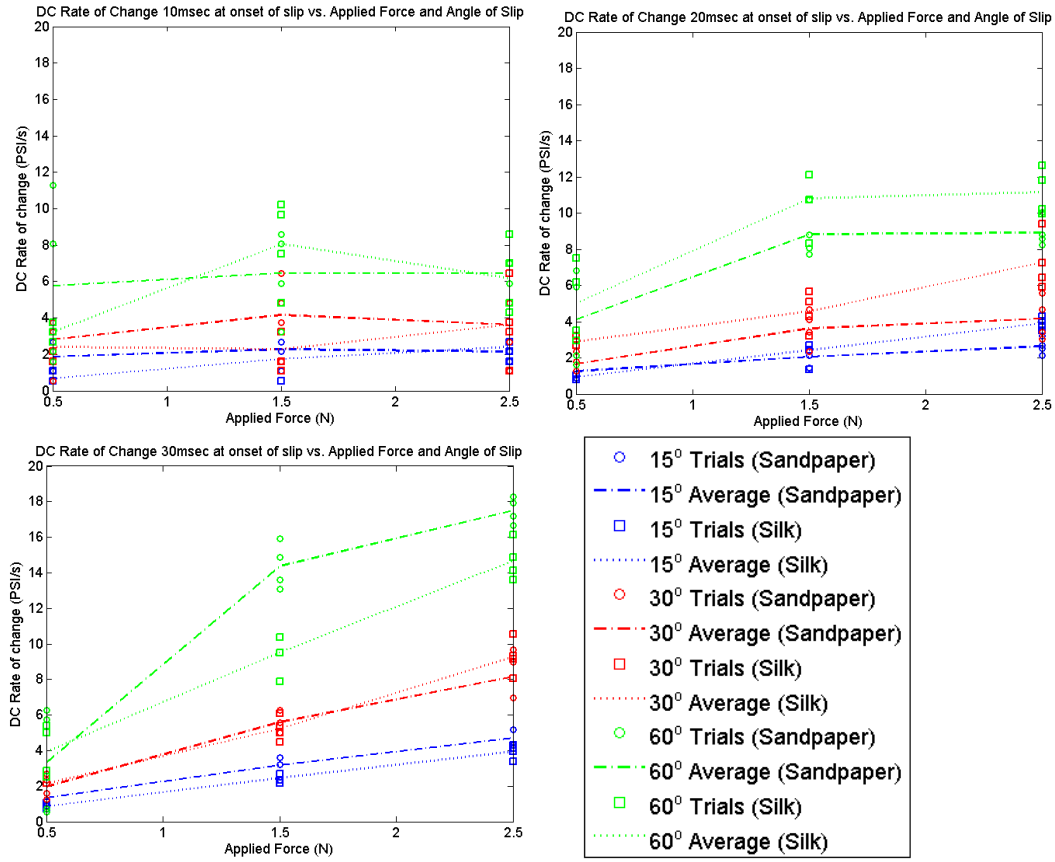
Figure 15. Rate of Change in DC Pressure at Onset of Slip. Unlike the trends found in the rate of AC pressure change, the case for 60° contact angle and 0.5N applied force was not significantly greater than for cases with different contact angles.

Electrode Impedance Assessment. Analyses performed on AC and DC pressure data yielded the same conclusion that lower forces and contact angles will be difficult to detect unless the threshold is significantly lowered. Analyses performed with impedance data may provide a solution to lower force and contact angle slip detection. An assessment was first performed to see the general trend of rate of change in impedance for each electrode. An arbitrary sampling window of 20 ms was first used. Figure 16 shows the average rate of change in impedance compared to all factors of interest. The electrode numbers were re-ordered with

21

respect the position along the y-axis on the XY-plane (Figure 9). Results indicated

that slippage caused significant drops in impedance value, specifically for

Electrode 7. The magnitude of the rate also increased as contact angle decreased

and applied force increased. This would make sense, since the slip created a

bulging effect on the skin that followed the direction of the slip. Contact angles of

15° and 30° resulted in greater contact surface area, which would increase the

likelihood of skin bulging. Furthermore, slips at low forces such as 0.5 N were

capable of inducing a rate of change in impedance of -2kΩ/s, which would

suggest that slips at low applied forces may potentially be detectable with the use

of electrode impedance data.

   To assess whether impedance information could be used to detect slip at

low contact angles and low applied forces, ratios between the rate of change in

Electrode 7 and the rate of change in Electrode 17 were compared for different

forces. For this assessment, I'_n denoted the rate of change in impedance for

electrode n. Electrode 17 was along the same x-axis as Electrode 7, and the results

from Figure 16 indicated that the values for Electrode 17 had remained consistent
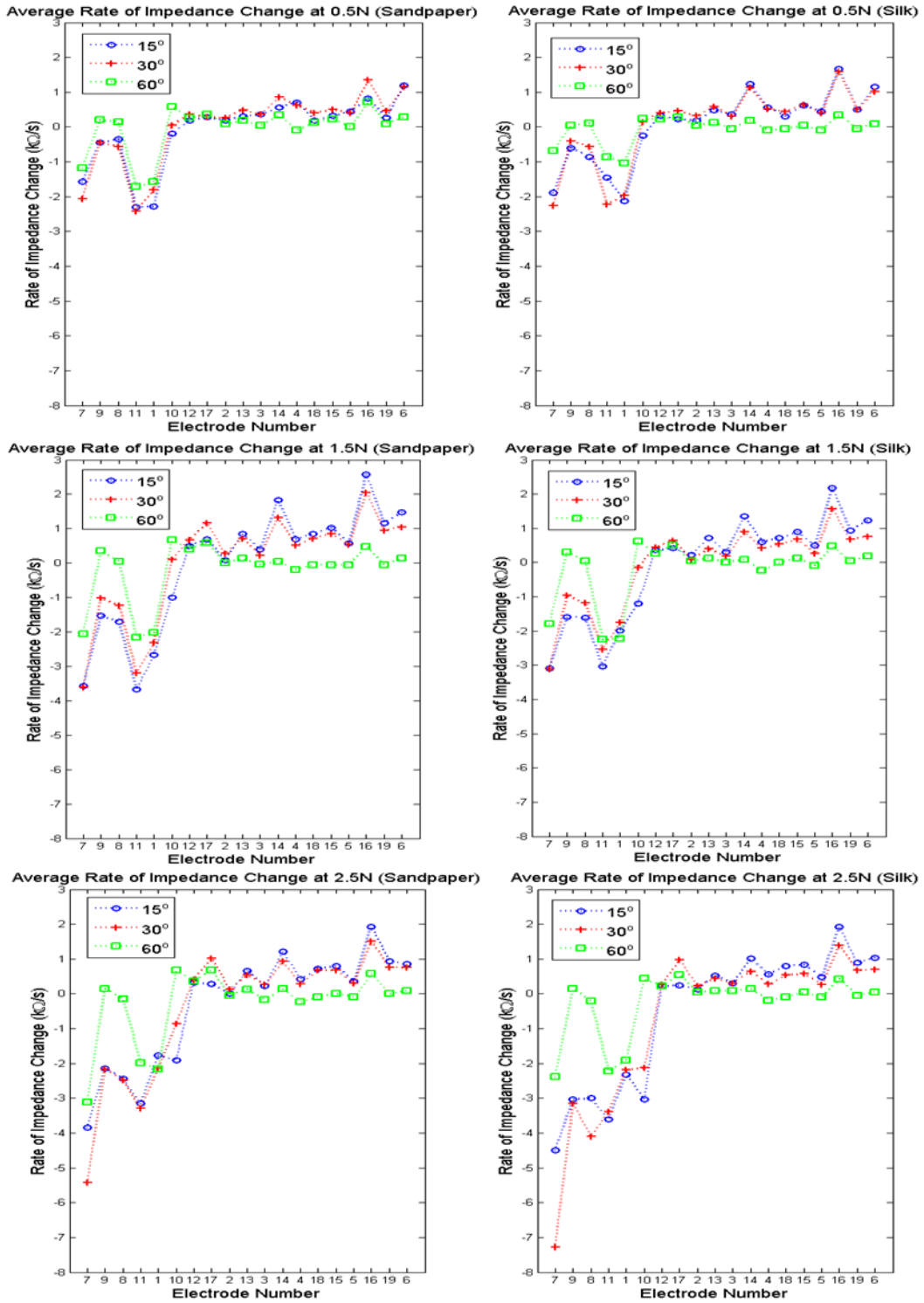
Figure 16. Average Rate of Change in Impedance at Various Applied Forces. A sampling window of 20 ms was used. One notable trend found was that lower contact angles exhibited greater rate of change in impedance for Electrode 7.

23

throughout the experiment. Different sampling windows were used to determine which time interval to use for future slip detection experiments. Figure 17 shows the average ratio between I'_7 and I'_{17}. Low forces appeared to exhibit large ratios compared to other forces. Using a 20 ms (2 sample points) sampling window seemed to provide the largest ratios for both sandpaper and silk. Prior tests suggested that a 30 ms sampling window showed greater magnitudes in the rate of change in impedance. However, information from ratio comparisons is more relevant for detecting slip direction, which showed that using a 20 ms sampling window resulted in greater magnitudes. Results indicate that applying a threshold of approximately -5 would allow for detection of all force levels for low contact angles.
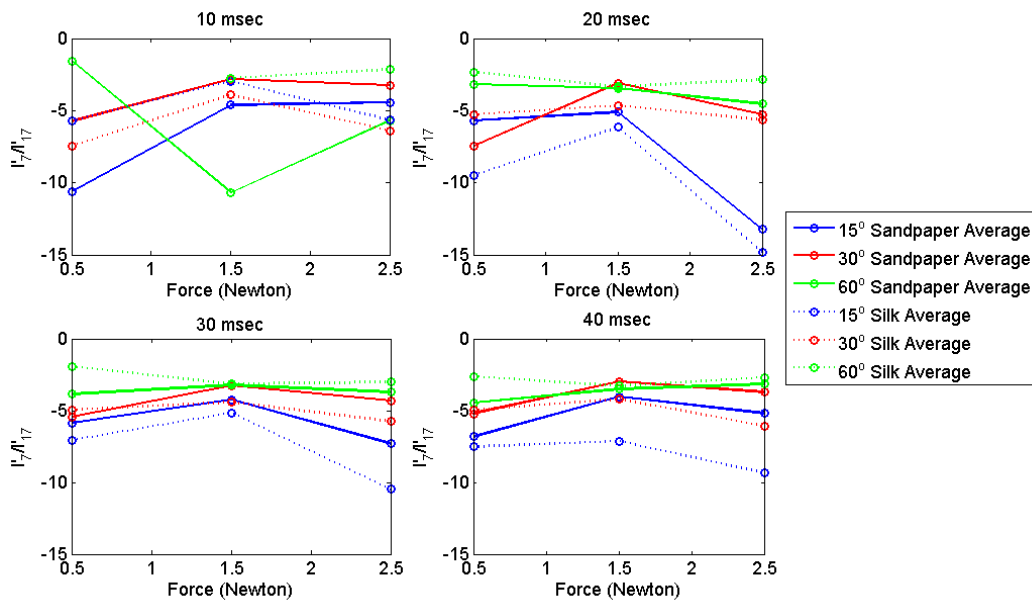
Figure 17. Ratio between the Rate Impedance Change of Electrode 7 and of 17. Low contact angles appear to exhibit the greatest ratio magnitude in all four sampling windows. A sampling window of 20 ms results in the largest difference in ratios when compared to other contact angles.

FUTURE WORK AND CONCLUSIONS

      AC Pressure Assessment. Results from AC pressure analysis indicated that applying a threshold could be helpful with detecting slips induced at both high applied force and contact angle. However, the threshold would have to be significantly lowered to accommodate lower force and contact angles. Nevertheless, a threshold could still be established to detect slip at more moderate levels of contact angle and applied forces in all AC pressure metrics. If rate of AC pressure change was used, the recommended sampling window would be 20 ms. Due to the findings found in the electrode impedance analysis, it would be advised that the threshold be set to detect slip induced from moderate to large applied forces and steep contact angles while slips induced by weaker applied forces and low contact angles be detected with electrode impedance data.

      DC Pressure Assessment. DC pressure and AC pressure exhibited the same trend, in which all metric responses increased when contact angle and force increased. Furthermore, the rate of DC pressure change was optimal with a 30 ms sampling window, whereas AC pressure was optimal at 20 ms. Thus, AC pressure metrics, more closely related to dynamic stimuli, would be favored for detection of slip as compared to DC pressure metrics. Additionally, AC pressure was sampled at a higher frequency (2200 Hz compared to 100 Hz), which may explain why a shorter AC pressure sampling window would suffice.

      Electrode Impedance Assessment. Results from electrode impedance data showed substantially large changes in impedance for low contact angles and low applied forces. Combined with the slip detection thresholds from AC pressure

data, it is possible to detect slip throughout the applied force and contact angle range. Furthermore, impedance data from sandpaper and silk textures appear to be very similar, suggesting that the proposed slip detection guidelines would hold for other textures as well.

Recommendation for Slip Detection. Since richer slip information was found at high contact angles and forces for AC and DC pressure but at low contact angles and forces for electrode data, it is recommended that future developments on slip detecting algorithms consider using multiple thresholds for different cases. For example, one could establish a threshold on the rate of AC pressure change to detect slip induced at higher fingertip forces and contact angles. A second threshold could be established on the ratio between I'_7 and I'_{17} to detect slip at lower fingertip forces and contact angles.

Future Studies on Non-slip Impacts. Throughout this experiment, much has been discussed about how to detect slip with data provided by the artificial finger. A key issue with establishing a threshold would be that non-slip perturbations, such as a taps or bumps, could also be registered as slips. Thus, future experiments could assess what effects non-slip perturbations have on the sensor data and determine which sensor information would be helpful in distinguishing non-slip perturbations from slip.

26

Chapter 2

PREDICTING THE DIRECTION OF SLIP DURING TWO-DIGIT GRASP

In a realistic scenario, haptic exploration of three dimensional objects would involve interactions with multiple digits that explore an object with different exploratory procedures (Lederman & Klatzky, 1987). The study presented in Chapter 1 only considered slip detection in one direction with a single tactile sensor. To better understand how slip information is encoded for multiple directions of slip and with two digits, it is critical to assess the feasibility of predicting slip direction with respect to two tactile sensors grasping an object with a precision pinch.

A study had shown that the latencies of grip-force responses to unpredictable loading forces vary with load direction in human subjects. These latencies were shorter when the object was pulled in more "dangerous directions" that would cause the subject to lose his/her grasp on the object (i.e., away from the palm and in the direction of gravity), regardless of hand position (Häger-Ross, Cole, & Johansson, 1996). Another study showed that grip responses were different when a gripped object was unexpectedly perturbed distally relative to the hand as opposed to proximally (Jones & Hunter, 1992). Thus, detecting the direction of slip with respect to body and gravity reference frames could be useful for developing context-dependent grip response algorithms for robotic hands and prosthetics. The following experiment was conducted to determine whether slip direction information can be extracted from two BioTac™ sensors.

MATERIALS AND METHODS

Robotic Hand and Instrumented Object. Two BioTac™ sensors were attached to the outermost digits of the three-fingered BarrettHand robotic hand. The BarrettHand digits were placed into a precision pinch posture with a flexion angle of 30° (Figure 18). A LabVIEW program controlled digit flexion. Throughout this experiment, the BioTac™ sensor on the robotic digit F1 ("index finger" of a right hand) will be referred to as "BioTac 1", and the BioTac™ sensor on the robotic digit F2 ("thumb" of a right hand) will be referred to as "BioTac 2". Furthermore, electrode numbering (fixed for each BioTac) was asymmetric when the artificial thumb and index finger were placed into the precision grip posture. In other words, Electrode 11 (see Figure 9) on BioTac 1 and Electrode 1 on BioTac 2 both point in the radial direction with respect to grasp, whereas Electrode 1 on BioTac 1 and Electrode 11 on BioTac 2 both point in the ulnar direction with respect to grasp. Thus, data that show mirrored or different slip responses between the two tactile sensors could potentially be useful for characterizing the direction of slip.
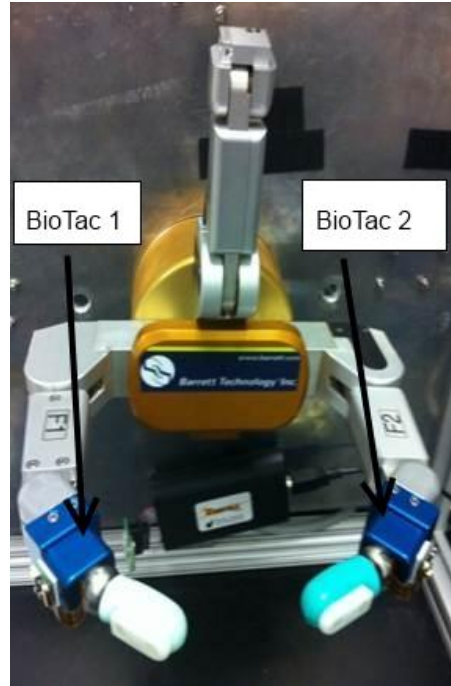
Figure 18. BarrettHand robotic hand outfitted with two BioTac™ tactile sensors.

The instrumented object that will be grasped by the robotic hand allows

for the monitoring of the grasp force (Figure 19). The instrument is comprised of

two circular parallel grip plates (3.5 in diameter, 0.125 in thick), an aluminum

housing for the load cells (see Appendix A1 and A2 for schematics), and the two

Nano-25 load cells. Modular circular plates can be interchanged in order to vary

the texture of the grip surface. The total mass of the object, including the texture

plate and load cells, was 290 grams, and the overall width was 1.5 inches.
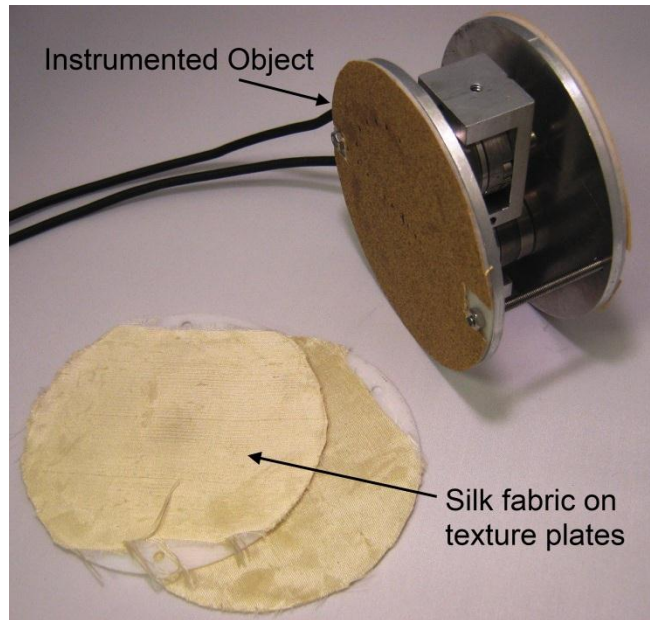
Figure 19. Instrumented Object with Texture Plates. The object consists of two load cells that measure the total grip force.

Data Acquisition. The experimental setup was designed to induce slip at the artificial fingertips by pulling the instrumented object away from robotic hand at different with respect to the ground (see Table 1 "Slip Scenario"). Prior to data collection, the object was first tethered to the aluminum chassis in order to prevent damage in case the object is dropped by the robot hand. Preliminary experiments revealed that the grasped object tends to fall off the planned slip trajectory and towards the ground while being dragged. Thus, in order to eliminate gravity as a confounding factor in this experiment, the object was tethered so that the robotic hand grasped the object at its center (Figure 20). The contact angle between the artificial finger and the parallel plates was approximately 62.5°, which means that the area of contact would be relatively small and that very few electrodes would be excited. Slip was induced by the DC motor by pulling on the instrumented object using an inextensible fishing line

(200 lbf monofilament line, Power Pro) that was attached to the threaded bar on the object (Figure 20). Data collection methods were identical to the experiment discuss in Chapter 1: each trial contained five seconds of BioTac™ sensor data with slip occurring two seconds after the onset of data collection.
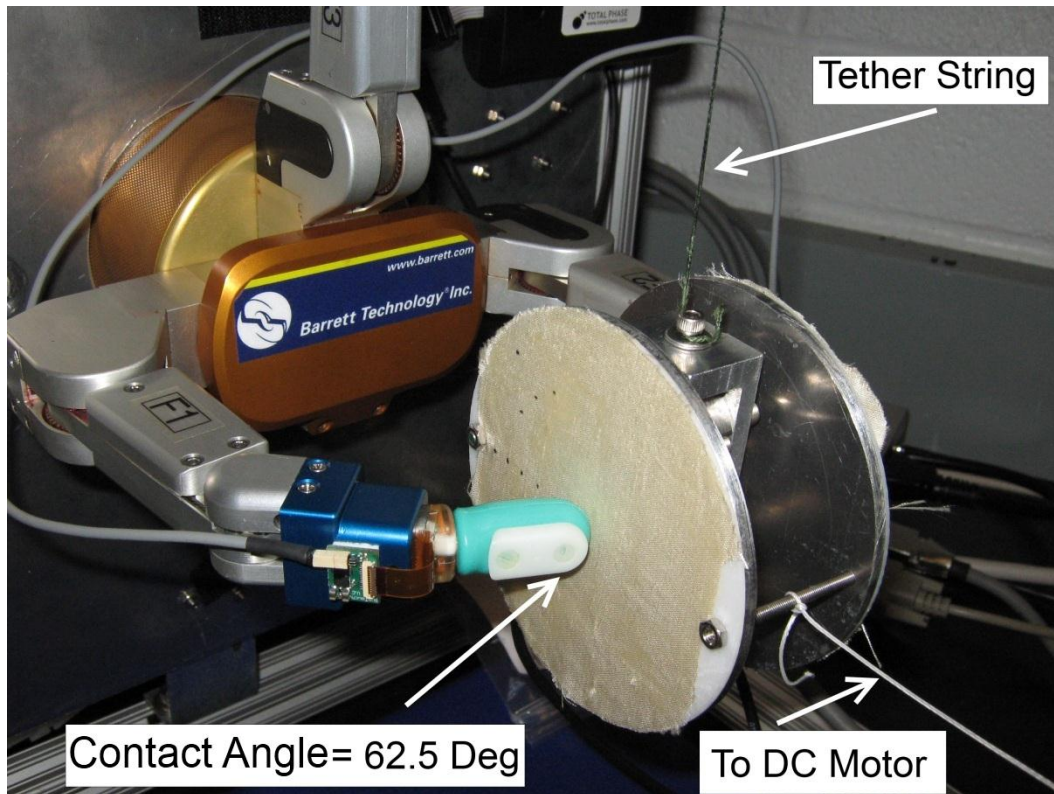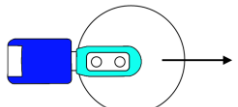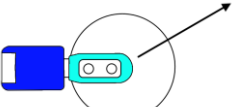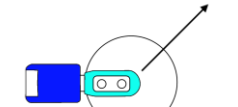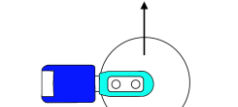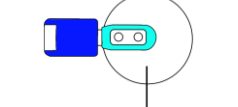
Figure 20. Experimental Setup. The DC motor drags the instrumented object away from the robotic hand at different slip angles.

Experimental Design. This experiment called for the testing of five different slip angles, three different applied grip (normal) forces, and two types of textures. The angle of slip was established to be the angle between the trajectory of the object and the ground plane, with slip towards the radial direction of the grasp was considered as positive. Thus, a -90° slip would result in the object

31

moving in the ulnar direction of the grasp (Table 2). Four trials were conducted

for each combination of slip angle, applied force, and texture type.

Table 2

Experimental Design for Determining the Direction of Slip

Slip Scenario	Slip Angle	Applied Grip Force (Per Finger)	Texture
	0°	0.75 N	150 Grit Sandpaper
	30°	1.25N	Silk
	45°	1.75N	
	90°		
	-90°		

Slip condition for all trials was fixed at 20 mm at 100mm/s. During the

experiment, grip forces of 1.5 N, 2.5 N, and 3.5 N (total across both fingertips)

were used. Based on the symmetry of the grasp, individual digit forces were

assumed to be half of the total grip forces. Data will be reported according to

individual digit grip forces of 0.75 N, 1.25 N, and 1.75 N for each BioTac™.

Data Analysis. Raw data from the BioTac™ sensor was converted to

physical units (e.g., psi, kΩ) according to the methods presented in Chapter 1.

Both pressure magnitude and rate of change in pressure at onset of slip for AC

and DC pressure were calculated. Sampling windows established in the previous experiment (20 ms for AC pressure, 30 ms for DC pressure, and 20 ms for electrode impedance) were used for the calculations of AC and DC pressure rates. The rate of change in impedance was also determined, along with a comparison with ratios between electrodes of interest. Three-dimensional plots were also generated with MATLAB to observe the rate of change in impedance with respect to the slip angle.

RESULTS AND DISCUSSION

Four trials were conducted for each combination of slip angle, applied force, and texture type except for combinations of 0.75 N and 1.25 N grip forces for the -90° slip direction. These combinations of experimental factors were not used for multiple reasons. First, it was realized that downward slips in the ulnar direction of grasp meant that the instrumented object could not be tethered to compensate for gravity. Furthermore, individual digit grip forces of 0.75N and 1.25N were insufficient for a stable grasp of the object in mid-air. Only a digit grip force of 1.75N was sufficient in keeping the object stationary. Thus, only trials with 1.75N applied force per digit were conducted for the -90° slip direction.

AC Pressure. A decrease in AC pressure magnitude occurred at the onset of slip following onset of slip still occurred for trials in this experiment. Figure 21 shows the pressure drop's magnitude compared to all factors of interest. It was noticed that increasing the slip angle caused a gradual decrease in the magnitude of the pressure drop. Additionally, an increase in digit grip force seemed to reduce

the effects of this trend. Slip induced at the 90° direction caused only a negligible pressure drop for both tactile sensors. Saturation at 0.1 psi was observed for digit grip forces of 1.25N and 1.75N.

Observing the AC pressure magnitude may not be useful for determining exact direction of slip, since both tactile sensors exhibit similar responses. This would make sense, since AC pressure is a just the result of the microvibrations caused by relative motion between the BioTac™ skin and textured plate. Because the BioTac™'s fingerprint is symmetric along the y-axis (see Figure 9, line at x = 0), slip in either the ulnar or radial direction would exhibit the same AC pressure response.
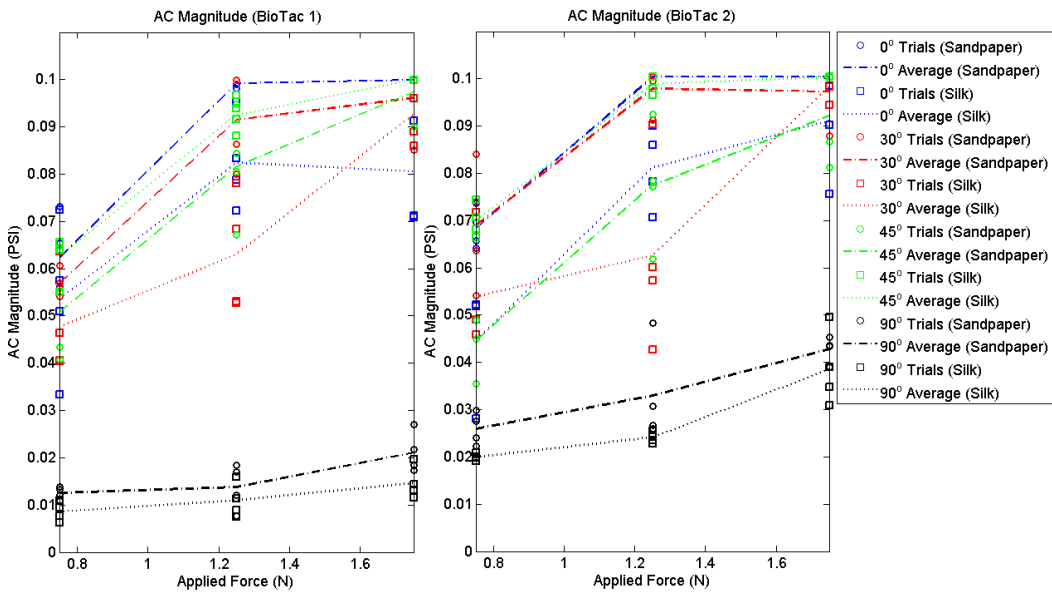
Figure 21. AC Magnitude of Both Sensors. The general trend showed that the AC pressure magnitude decreased in magnitude as slip angle and grip force increased.

The rate of AC pressure also decreased in magnitude as slip angle and grip force increased (Figure 22). As the slip angle increases, the general rate of change

in pressure decreases. An increase in applied force did not seem to mitigate this trend. Additionally, both fingers appear to exhibit similar rate values. As a result, observing the rate of AC pressure change may not be a viable metric for detecting the exact direction of slip. However, it may serve as an indicator for the absolute slip angle. Given that the rate of change in pressure is affected by both the direction of slip and the amount of applied force, it is possible to create a statistical model that may predict how many degrees has a slip deviated from a $0°$ slip. This would require additional trials as well as factor levels.

Based on the results found in the previous experiment, it is possible to utilize one mode of sensing to detect slip within a range of cases and utilize another metric to detect slip within a different range of cases. For example, setting a rate of AC pressure change threshold at -1 psi/s could still be used to detect slip for cases with slip angles less than or equal to $45°$. Consequently, it is hoped that another feature such as DC pressure or electrode impedance would be used to detect slip for steeper direction angles.
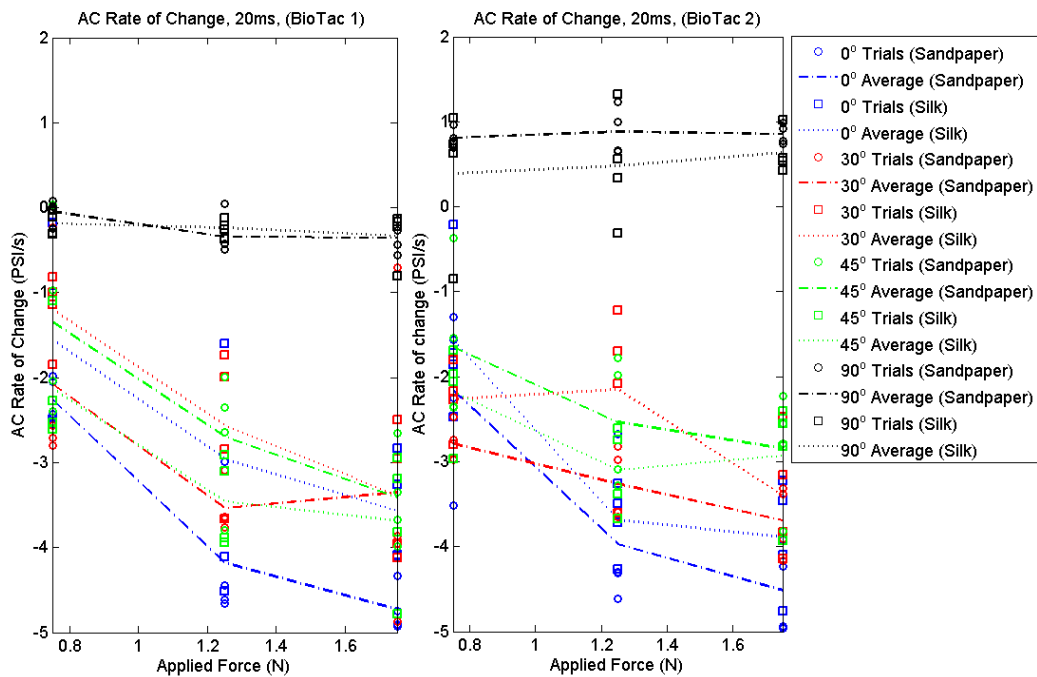
Figure 22. Rate of Change in AC Pressure of Both Sensors. The general trend also shows that the response decreases in magnitude as slip angle increases.

DC Pressure. Analysis of DC pressure magnitude and rate of DC pressure change revealed trends similar to those found in the AC pressure assessment. Figure 23 shows DC magnitude compared to all factors of interest, and Figure 24 shows the rate of change in DC pressure compared to all factors of interest. Results from both figures show a general trend where an increase in the slip angle tends to reduce the DC magnitude as well as rate of change in pressure. Additionally, information from both BioTac™ sensors appears to follow the same trend, so prediction of slip direction in the plane of the grip surface would also not be possible. Nevertheless, the same approach for AC pressure assessment can be applied to DC pressure. Based on the trends observed, a model can be developed

36

for predicting the slip angle if given the applied force and rate or magnitude response.

The rate of DC pressure change may be a useful metric for slip detection. Establishing a rate threshold at 2 psi/s would be effective for predicting slip within the range of the tested force and slip angles between 0° and 45°. Overall, results from AC and DC pressure analyses showed that inter-digit (across multiple digits) differences in pressure responses were minimal because of the symmetry of the grasp and the slip stimulus with respect to the grasp. Thus, inter-digit comparisons for AC pressure or DC pressure would not be very useful for predicting the direction of slip. Furthermore, since only one channel of data was available in each sensor for measuring AC or DC pressure, intra-digit (within a single digit) comparisons would not be possible for each of these datastreams.
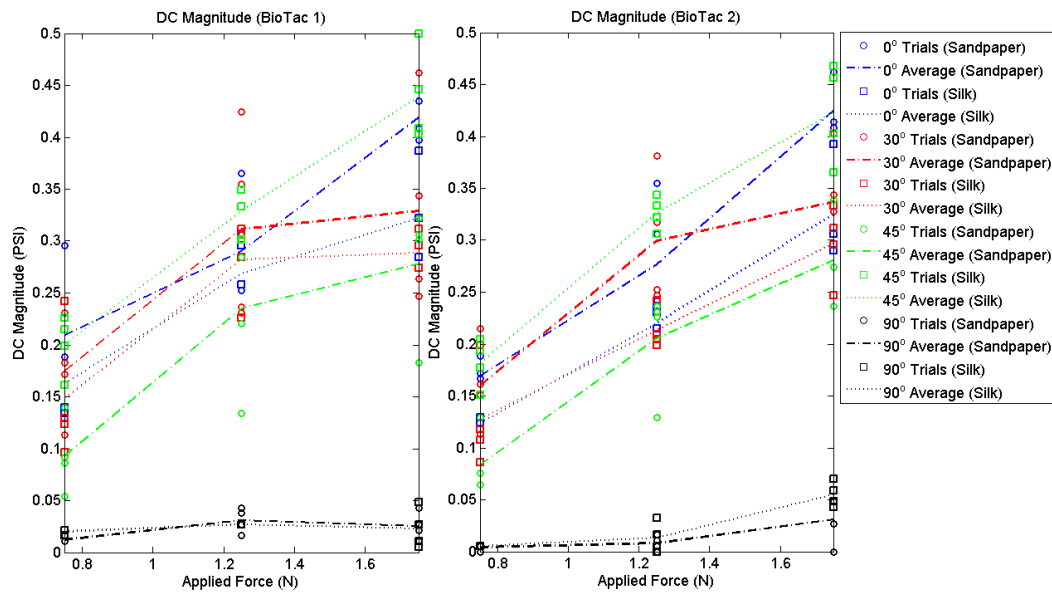
Figure 23. DC Magnitude of Both Sensors. 45° silk trials appear to deviate from the general trend, but the rest of the slip angle trials follow the pattern.

37
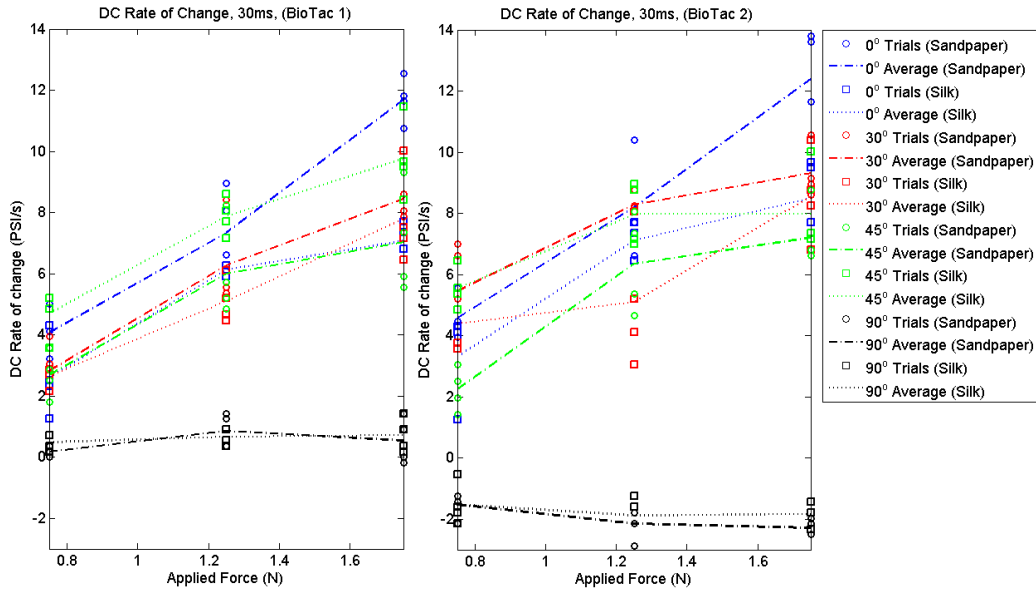
Figure 24. Rate of Change in DC Pressure of Both Sensors. A threshold 2 psi/s could be used to detect slip for slip angles between 0° and 45°. Responses in 90° trials appear to be different for the two sensors, but the trend that increasing slip angle resulted in a decrease in DC rate of change was still present.

Electrode Impedance. Analysis of electrode impedance data suggest that the direction of slip is encoded in the slow-adapting electrode data. Figure 25 shows the average rate of change in impedance at the onset of slip for an applied force of 1.25N for each electrode. The top two graphs are from BioTac 1, and the bottom two graphs are from BioTac 2. The rate of change in impedance was observed to be mirrored between BioTac 1 and BioTac 2.
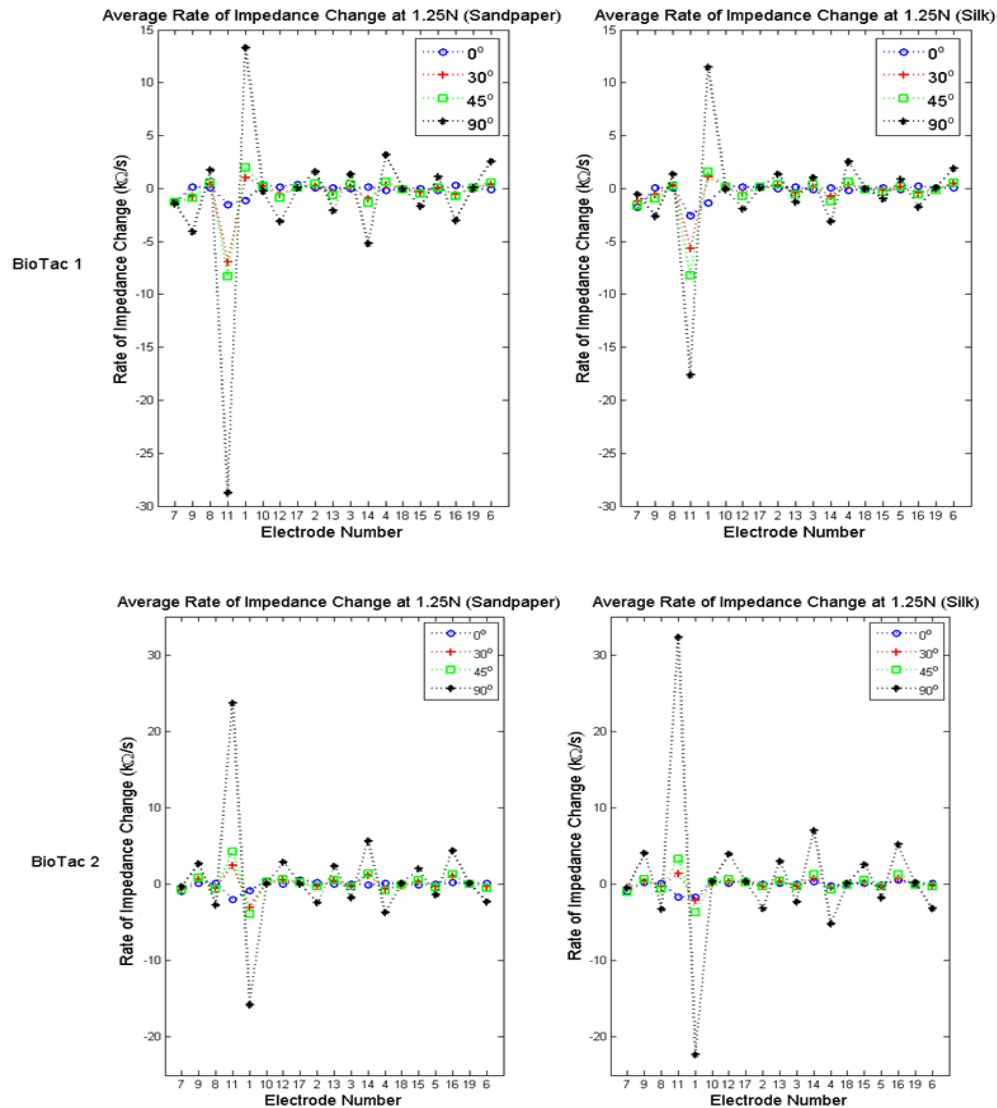
Figure 25. Average Rate of Change in Impedance at 1.25N for Both Sensors. The rate of change in impedance are opposite in sign for the two sensors, which is expected.

Since the spatial location of the electrodes on the surface of the BioTac™ core was both known and constant, it was possible to leverage the unique spatiotemporal changes in each electrode in order to determine the actual direction of slip. The following Figure 26 show a 3D plot of the rate of change in impedance for both fingers. The coordinates for the electrodes were the same ones

used in Figure 9. Increasing the slip angle resulted in a greater drop in rate of change in impedance at Electrode 11 for BioTac 1 and at Electrode 1 for BioTac 2. This would make sense, since slipping would induce a bulge on the skin and, thus, lower the impedance measurement. Conversely, a -90° slip angle resulted in a significant rise in the rate of change in impedance at Electrode 11 for BioTac 1 and at Electrode 1 for BioTac 2. This would also make sense, since a -90° would pull the artificial skin in the ulnar direction of the grasp while increasing the compression between the electrodes and the skin, resulting in greater impedance.
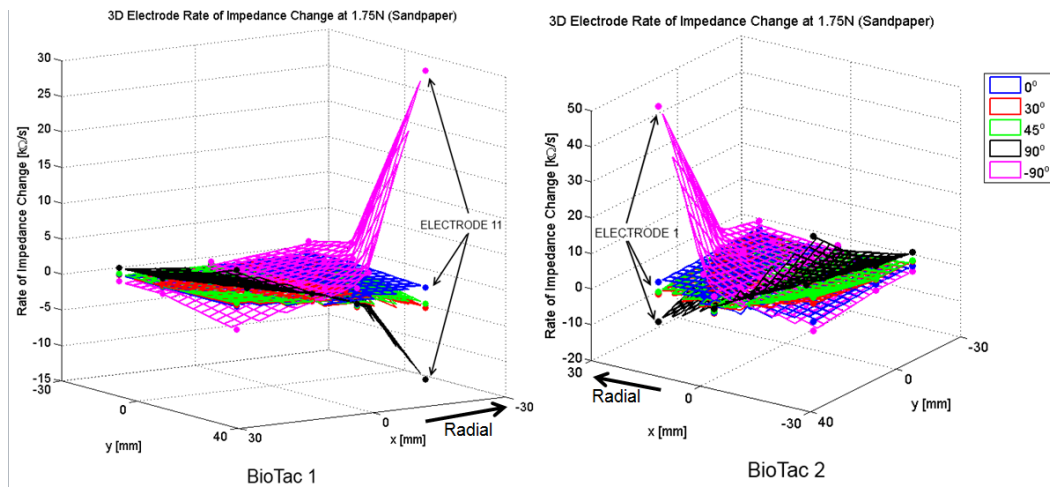
Figure 26. 3D Plots of the Rate of Change in Impedance at 1.75N for Both Sensors. The 30° case exhibited a greater rate of change in impedance than the 45° case.

The rate of change in impedance for Electrodes 11 and 1 may be useful for detecting ±90° slips. However, this would not address the issue of determining other slip angles in between -90° and 90°. One proposed solution would be to compare the ratio between the radial and ulnar electrodes (Electrode 11 and 1) within a single BioTac™ to the electrode at the tip of the finger (Electrode 7). Theoretically, the ratio between the rate of change from the radial or ulnar

electrodes and the electrode at the fingertip would be proportional to the slip angle.

Figure 27 shows the various ratios conducted for both tactile sensors. The plots represent the average ratio for different applied forces plotted against their slip angles. The general trend was that the ratio between electrodes at the radial aspect of the grasp and at the tip would be positive for radial directions of slip and negative for ulnar directions of slip. Similarly, results also show that the opposite trend also holds: the ratio between electrodes at the ulnar aspect of the grasp and at the tip would be negative for radial directions of slip and positive for ulnar directions of slip. No useful trends were noted for the ratio between impedance rate from the radial and ulnar electrodes (shown by I'_1/I'_{11} and I'_{11}/I'_1 in Figure 27).

For example, as the slip angle increased for BioTac 1, the ratio between the response from Electrode 11 and Electrode 7 increased, whereas the ratio between the response from Electrode 1 and Electrode 7 decreased. Conversely, as the slip angle increased for BioTac 2, the ratio between the response from Electrode 1 and Electrode 7 also increased, whereas the ratio between the response from Electrode 11 and Electrode 7 decreased. With more tests done on different slip angles, it may be possible to create a model that relates specific electrode ratios to the slip angle in both radial and ulnar directions. This model could include fingertip force as well as the impedance ratios as input variables to determine slip direction. Ultimately, results clearly indicate that intra-digit spatiotemporal metrics for the electrode data (from all 19 channels) such as ratios

41

could provide valuable information for detecting slip direction. Detecting slip at steeper slip angles could be done by establishing a threshold in which any ratio that surpasses it would indicate that slip had occurred. The current model does not have enough data points to support this metric, but it is hoped that future experiments would consider this method for slip detection.
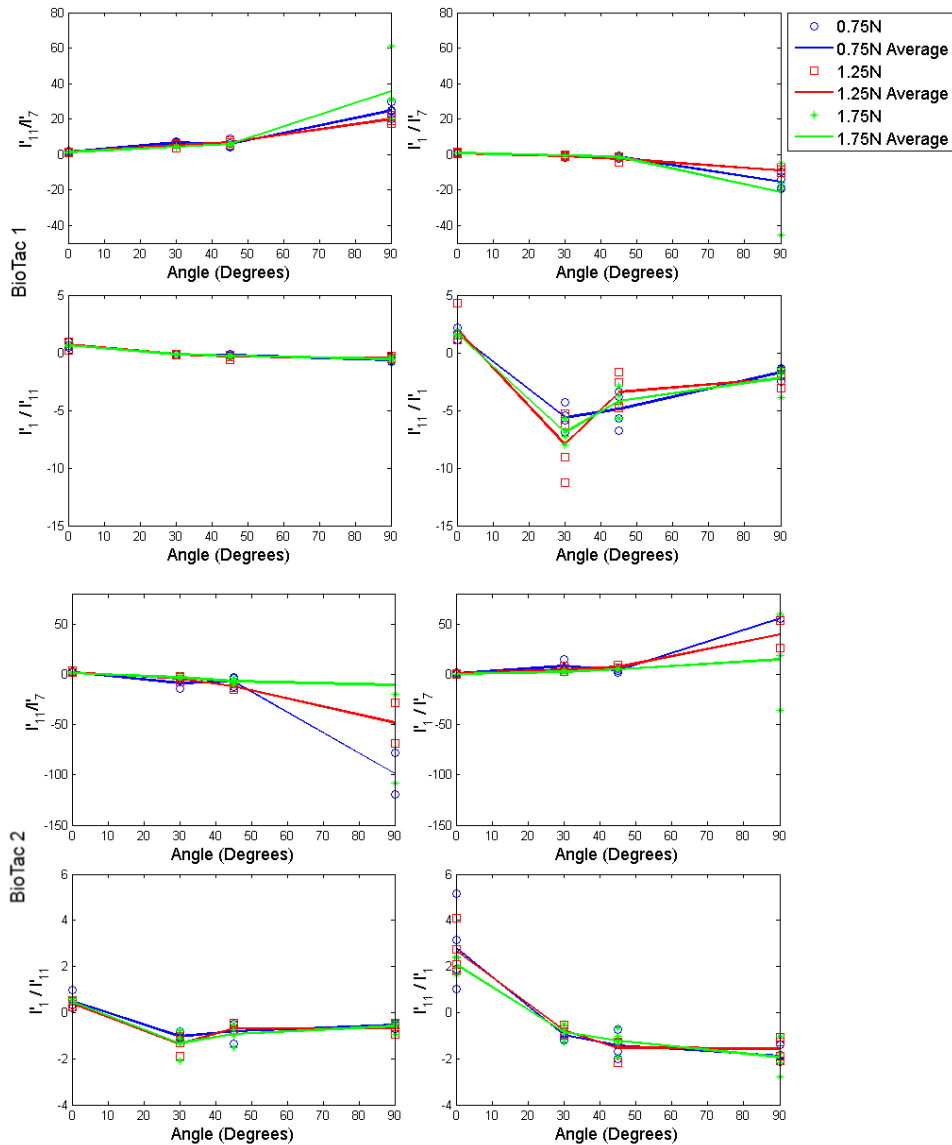

Figure 27. Ratios between radial-ulnar electrodes and tip electrodes for Both Sensors. The ratio between the radial and ulnar electrodes for both sensors did not appear to provide useful information.

FUTURE WORK AND CONCLUSIONS

      AC and DC Pressure Analysis. Results clearly indicated that the magnitude and rate of change from both AC and DC pressure data attenuated as the direction of slip increased (i.e., as the radial component of the slip trajectory increased). For both AC and DC pressure, both tactile sensors exhibited similar responses, which meant that neither mode of sensing would be useful for determining the direction of slip. It was mentioned that AC and DC pressure data could still be used to determine the absolute slip angle. However, this was based on the assumption that a strong linear relationship existed between pressure responses and applied force as well as slip angle. That is, at a known applied force, the pressure response would be the result of only one specific angle. Without prior knowledge of the applied force, slip direction would not be determinable from pressure data alone. Consequently, further investigation would be necessary to properly assess whether or not a hydrophone alone would be useful for predicting slip direction at an artificial finger.

      Binary measure of slip, on the other hand, could still be achievable by applying a threshold. In this case, decreasing the threshold would increase the chance for predicting slip at steeper slip angle. However, it should be noted that decreasing the threshold may increase the likelihood of detecting false positives. Trials at additional factor levels, such as grip forces greater than 1.75 N and slip angles greater than 45°, are recommended to better understand the effects of applied force and direction of slip on the pressure data. A better understanding of the effects would allow for selection of robust slip detection thresholds.

Electrode Impedance Analysis. Electrode impedance data showed the most promise in predicting slip direction by comparing ratios of impedance change between electrodes in the radial aspect of the grasp and electrodes at the tip. This was because the electrode data obtained by the two sensors was different due to their asymmetric spatial locations with respect to the radial and ulnar directions of the precision pinch grasp. So far only four different slip angles were tested. To properly assess the feasibility of impedance data and establish a function that relates electrode impedance ratios to slip angle, additional slip angles must be tested. Furthermore, the current experimental setup limits the number of electrodes that can be stimulated due to the high contact angle and resulting low contact area. Grasping the instrumented object at a lower contact angle may provide additional information for predicting slip angles because contact area would decrease and more impedance electrodes in the array would be affected by changes in the finger-object interactions. Increasing grip force could also serve to amplify vibrations due to slip.

Recommendation for Slip Detection and Angle Prediction. At this moment, it is advised that one utilize electrode impedance data, and intra-digit ratios of electrode impedance measurements, to predict the slip angle. Inter-digit differences in AC and DC pressure data were minimal because of the symmetry of the grasp and the slip stimulus with respect to the grasp. Thus, intra-digit comparisons for either AC pressure or DC pressure would not be useful for predicting slip direction. Angle prediction algorithms should consider the ratio between the electrode on the radial (or ulnar) aspect of the grasp and the electrode

44

on the tip of the artificial finger, and then map the ratios to their respective slip angles. A model could then be created that relates the electrode impedance ratio to slip angle. For slip detection, it is recommended that thresholds based on the rate of AC and DC pressure change be used to detect slip for low slip angles (primarily slip in the distal direction of the grasp) and thresholds based on the electrode impedance ratio be used to detect slip for high slip angles (primarily slip in the radial or ulnar direction of the grasp).

Recommended Changes to Experimental Setup. When collecting data on slips occurring with sandpaper texture, it was noted that the skin on the tactile sensor began to show signs of wear. This wear may have affected the sensor data slightly. Routine skin replacement may be necessary in order to obtain consistent slip data. Furthermore, the output of the load cells varied by ±0.5N and often required adjustments for bias. Annual calibration is likely necessary to minimize variability in grip force measurements.

Regarding the instrumented object itself, it has been noted that over-tightening the crossbars that connect to the inextensible string can affect the grasp force readings. The current solution is to ensure that the screws on the bars are loose enough to ensure that no additional compression was added to the instrumented object. Future considerations would be to use another method for attaching the string to the object without affecting the load cell readings. Another issue found was that the instrumented object may have been slipping more towards one BioTac™ than the other, which would affect the information

acquired from both sensors. This might explain the discrepancy in the data found for the 90° slips in AC and DC pressure (Figures 21, 22, 23 and 24).

The current experimental setup only allows for prediction based on case-specific models. Future work could consider a multivariate analysis approach for detecting slip and predicting slip direction. A multivariate analysis approach might enable the development of a comprehensive slip detection model that encompasses all relevant variables such as fingertip force, contact angle, etc. Another approach to developing a slip detection model would be to apply real-time machine learning algorithms to classify slip onset as well as slip direction. Real-time machine learning could allow for continuous model refinement, but would require more computational power. Nevertheless, this study demonstrates that developing a multi-directional slip detection model is certainly viable using multimodal BioTac™ sensor data.

REFERENCES

Cole, K. J., & Abbs, J. H. (1988). Grip force adjustments evoked by load force perturbations of a grasped object. *J Neurophysiol*, *60*(4), 1513–1522.

Fishel, J. A., Santos, V. J., & Loeb, G. E. (2008). A robust micro-vibration sensor for biomimetic fingertips. *Biomedical Robotics and Biomechatronics, 2008. BioRob 2008. 2nd IEEE RAS & EMBS International Conference on* (pp. 659–663). Presented at the Biomedical Robotics and Biomechatronics, 2008. BioRob 2008. 2nd IEEE RAS & EMBS International Conference on. doi:10.1109/BIOROB.2008.4762917

Häger-Ross, C., Cole, K. J., & Johansson, R. S. (1996). Grip-force responses to unanticipated object loading: load direction reveals body- and gravity-referenced intrinsic task variables. *Experimental Brain Research*, *110*(1), 142–150. doi:10.1007/BF00241383

Hsia, A. (2011). Use of a hydrophone to detect slip between an artifical fingertip and a grasped object. *Proceedings of Fulton Undergraduate Research Symposium*.

Johansson, R. S., & Flanagan, J. R. (2008). Tactile sensory control of object manipulation in humans. In J. H. Kaas & E. Gardner (Eds.), *Handbook of the Senses* (Vol. 6: Somatosensation, pp. 67–86). San Diego: Academic Press. Retrieved from http://umu.diva-portal.org/smash/record.jsf?searchId=1&pid=diva2:208419

Jones, L. A., & Hunter, I. W. (1992). Changes in pinch force with bidirectional load forces. *Journal of Motor Behavior*, *24*(2), 157–164.

Lederman, S. J., & Klatzky, R. L. (1987). Hand movements: a window into haptic object recognition. *Cognitive Psychology*, *19*(3), 342–368.

Mountcastle, V. B., LaMotte, R. H., & Carli, G. (1972). Detection thresholds for stimuli in humans and monkeys: comparison with threshold events in mechanoreceptive afferent nerve fibers innervating the monkey hand. *J Neurophysiol*, *35*(1), 122–136.

Purves, D. (2001). *Neuroscience* (2nd ed.). Sunderland(MA): Sinauer Associates.

Syntouch - Technology Overview. Retrieved April 7, 2012, from http://www.syntouchllc.com/Technology/TechnologyOverview.php

Wettels, N., & Loeb, G. E. (2011). Haptic Feature Extraction from a Biomimetic Tactile Sensor: Force, Contact Location and Curvature.

Wettels, N., Parnandi, A. R., Ji-Hyun Moon, Loeb, G. E., & Sukhatme, G. S. (2009). Grip Control Using Biomimetic Tactile Sensing Systems. *Mechatronics, IEEE/ASME Transactions on*, *14*(6), 718–723. doi:10.1109/TMECH.2009.2032686

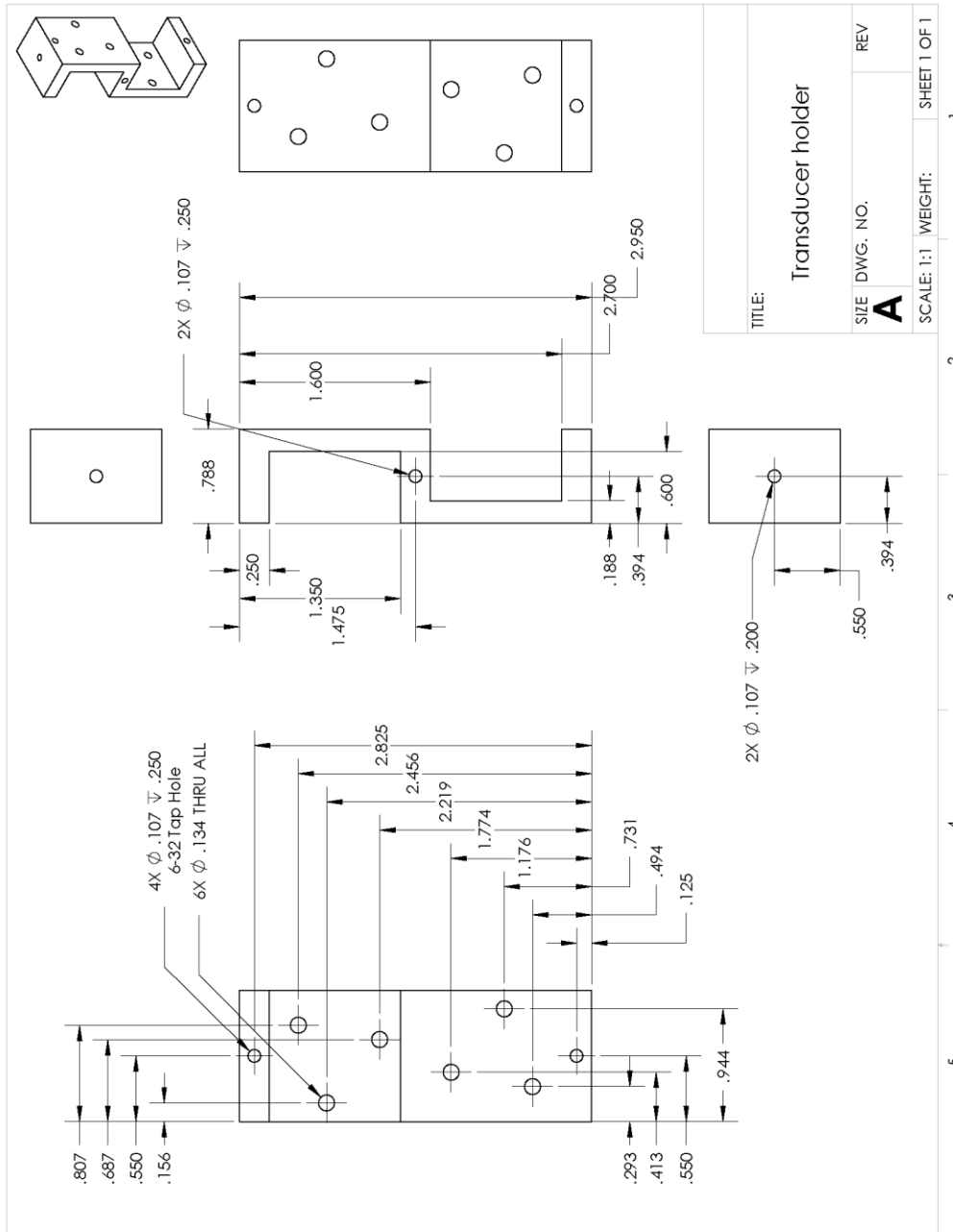Wettels, Nicholas. (2011, May). *Biomimetic tactile sensor for object identification and grasp control* (PhD dissertation). University of Southern California, Los Angeles, CA.

APPENDIX A

SCHEMATICS FOR INSTRUMENTED OBJECT COMPONENTS
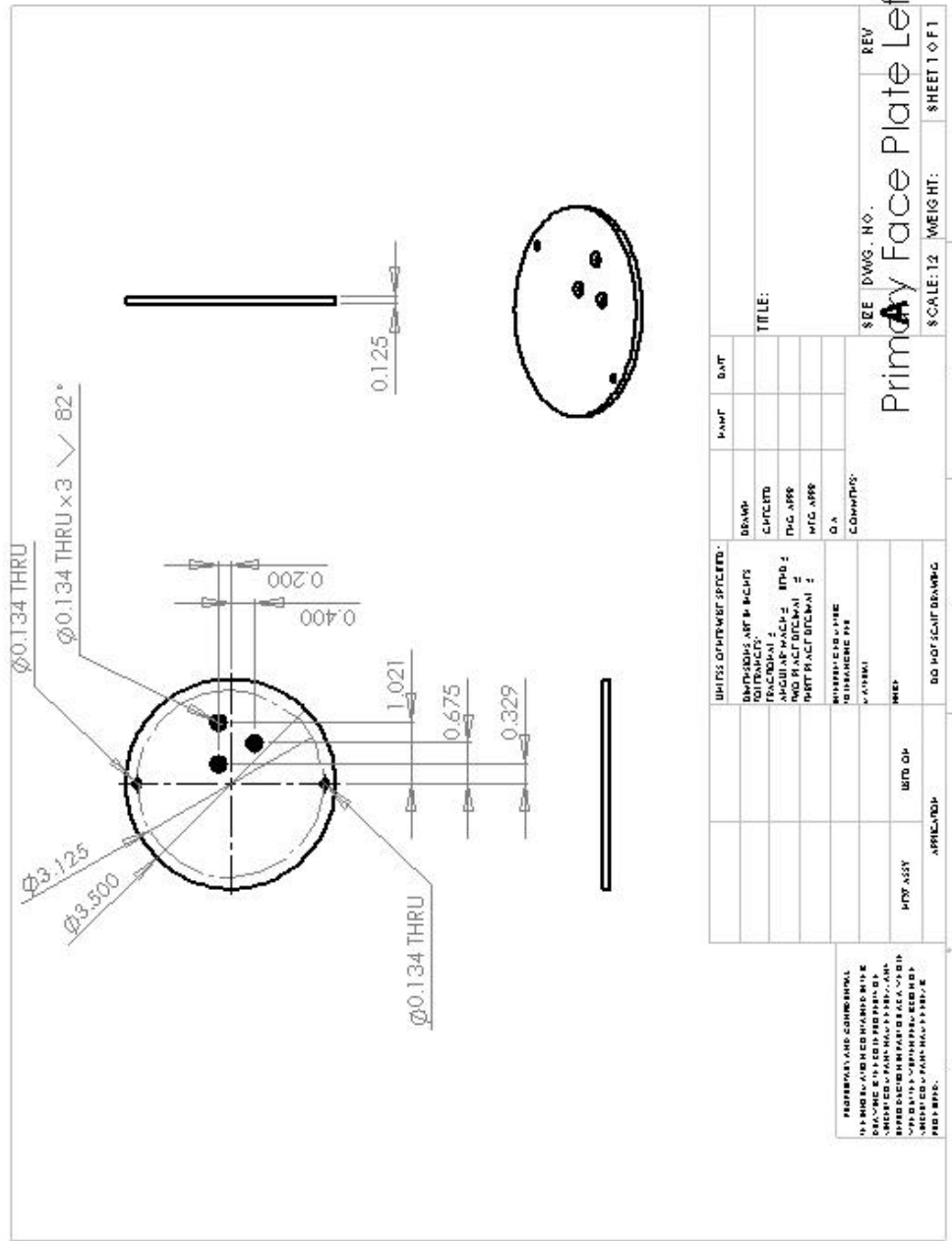
A1. Schematic for the Instrumented Object's Contact Plates.

A2. Schematic of the Instrumented Object's Central Frame for Transducer Attachment.

APPENDIX B

RELEVANT MATLAB CODE

Note: For brevity, the MATLAB code that follows is the relevant subset of the complete code used for data collection and analysis.

The following code is used for studies in both Chapter 1 and 2.

```
% AC and DC Magnitude and Rate of Pressure Change Calculation
for i = 1:36
    load(char(FileNames(i)));
Magnitude(i) = abs(min(Pac_1));
DC_Magnitude(i) = max(Pdc_1)-Pdc_1(1);
Sandpaper1Change(i) = (Pac_1((SandpaperOnset(i)+1)*22)-Pac_1(SandpaperOnset(i)*22))/0.01;
DC_Sandpaper2Change(i) = (Pdc_1(SandpaperOnset(i)+2)-Pdc_1(SandpaperOnset(i)))/0.02;

% Rate of Electrode Impedance Change Calculation (Each sample point is 10 ms, so divide by
corresponding time).  For example,
    ElectrodeAnalysis2(k,i) = (electrodes_1(SandpaperOnset(i)+2,k)-
electrodes_1(SandpaperOnset(i),k))/0.02;
end


% Rearranging Electrodes array in order of position on the finger (Electrode 7 is on the tip, so first
value in array)
ElectrodeSorting(1,:) = ElectrodeAnalysis(7,:);
ElectrodeSorting(2,:) = ElectrodeAnalysis(9,:);
ElectrodeSorting(3,:) = ElectrodeAnalysis(8,:);
ElectrodeSorting(4,:) = ElectrodeAnalysis(11,:);
ElectrodeSorting(5,:) = ElectrodeAnalysis(1,:);
ElectrodeSorting(6,:) = ElectrodeAnalysis(10,:);
ElectrodeSorting(7,:) = ElectrodeAnalysis(12,:);
ElectrodeSorting(8,:) = ElectrodeAnalysis(17,:);
ElectrodeSorting(9,:) = ElectrodeAnalysis(2,:);
ElectrodeSorting(10,:) = ElectrodeAnalysis(13,:);
ElectrodeSorting(11,:) = ElectrodeAnalysis(3,:);
ElectrodeSorting(12,:) = ElectrodeAnalysis(14,:);
ElectrodeSorting(13,:) = ElectrodeAnalysis(4,:);
ElectrodeSorting(14,:) = ElectrodeAnalysis(18,:);
ElectrodeSorting(15,:) = ElectrodeAnalysis(15,:);
ElectrodeSorting(16,:) = ElectrodeAnalysis(5,:);
ElectrodeSorting(17,:) = ElectrodeAnalysis(16,:);
ElectrodeSorting(18,:) = ElectrodeAnalysis(19,:);
ElectrodeSorting(19,:) = ElectrodeAnalysis(6,:);
for k = 1:9
    meanSort(:,k) = mean(ElectrodeSorting(:,((4*k)-3):k*4),2);
end


% Averaging magnitudes and rates of change for plotting purposes
Average = [mean(Magnitude(1:4)) mean(Magnitude(5:8)) mean(Magnitude(9:12)) ...
    mean(Magnitude(13:16)) mean(Magnitude(17:20)) mean(Magnitude(21:24)) ...
    mean(Magnitude(25:28)) mean(Magnitude(29:32)) mean(Magnitude(33:36))];
Sandpaper1ChangeAverage = [mean(Sandpaper1Change(1:4)) mean(Sandpaper1Change(5:8))
mean(Sandpaper1Change(9:12)) ...
    mean(Sandpaper1Change(13:16)) mean(Sandpaper1Change(17:20))
mean(Sandpaper1Change(21:24)) ...
```

```
            mean(Sandpaper1Change(25:28)) mean(Sandpaper1Change(29:32))
mean(Sandpaper1Change(33:36))];


DC_SandAverage = [mean(DC_Magnitude(1:4)) mean(DC_Magnitude(5:8))
mean(DC_Magnitude(9:12)) ...
   mean(DC_Magnitude(13:16)) mean(DC_Magnitude(17:20)) mean(DC_Magnitude(21:24)) ...
   mean(DC_Magnitude(25:28)) mean(DC_Magnitude(29:32)) mean(DC_Magnitude(33:36))];
DC_Sandpaper1ChangeAverage = [mean(DC_Sandpaper1Change(1:4))
mean(DC_Sandpaper1Change(5:8)) mean(DC_Sandpaper1Change(9:12)) ...
   mean(DC_Sandpaper1Change(13:16)) mean(DC_Sandpaper1Change(17:20))
mean(DC_Sandpaper1Change(21:24)) ...
   mean(DC_Sandpaper1Change(25:28)) mean(DC_Sandpaper1Change(29:32))
mean(DC_Sandpaper1Change(33:36))];
```

The following subset of code was used solely for the work presented in Chapter 1.

```
% Ratio Calculations for Force = 0.5N, Angle = 15, I7/I17
RatioValues(1) = meanSort(1,1)/meanSort(8,1);
   RatioValues(2) = meanSort(1,2)/meanSort(8,2);
   RatioValues(3) = meanSort(1,3)/meanSort(10,3);
```

The following subset of code was used solely for the work presented in Chapter 2.

```
%Ratio Test Code%

%Sandpaper, Vary by Force
%Ratio of Impedance 11 to 7 for 0 Degree, FORCE = 0.75N
for i = 1:4
   a(i) = ElectrodeSorting2(4,i)/ElectrodeSorting2(1,i);
end
%Ratio of Impedance 11 to 7 for  30 Degree
for i = 5:8
   a(i) = ElectrodeSorting2(4,i+8)/ElectrodeSorting2(1,i+8);
end
%Ratio of Impedance 11 to 7 for 45 Degree
for i = 9:12
   a(i) = ElectrodeSorting2(4,i+14)/ElectrodeSorting2(1,i+14);
end
%Ratio of Impedance 11 to 7 for 90 Degree
for i = 13:16
a(i) = ElectrodeSorting2(4,i+24)/ElectrodeSorting2(1,i+24);
end
```

The following code was adapted from code provided by Syntouch LLC. The code preprocesses raw data into meaningful data having relevant physical units (e.g., psi or kΩ).

```matlab
% Data Preprocessing Code%

function TransformCodev2(DataFileName,BaselineFileName)

% loading data from the Cheetah File
data = importdata(DataFileName);
baseline_data = importdata(BaselineFileName);

%% AC Pressure

% retrieving the AC Pressure data
Pac_sampling_freq = 2200;
num_of_Pac_readings = length(data(:,1))/2;
Pac_time_end = num_of_Pac_readings/Pac_sampling_freq;
Pac_time = linspace(0, Pac_time_end-(1/Pac_sampling_freq), num_of_Pac_readings);

% signals from different BioTacs
Pac_1 = data(2:2:length(data(:,5)), 5);
Pac_2 = data(2:2:length(data(:,7)), 7);

Baseline_Pac_1 = baseline_data(2:2:length(baseline_data(:,5)), 5);
Baseline_Pac_2 = baseline_data(2:2:length(baseline_data(:,7)), 7);

% Transform AC pressure to psi
% x_midline is signal at rest, use mean of values from 2-3s

x_midline1 = mean(Baseline_Pac_1);
x_midline2 = mean(Baseline_Pac_2);

Pac_1 = (Pac_1-x_midline1).*54.211762*10^-6;
Pac_2 = (Pac_2-x_midline2).*54.211762*10^-6;

%% Electrodes

% retrieving the electrodes' data
electrodes_sampling_freq = 100;
interval = 44;

% signals from the different BioTacs
for k = 1:19
    electrodes_1(:,k) = data( (2*k)-1 : interval : end, 5);
    electrodes_2(:,k) = data( (2*k)-1 : interval : end, 7);

    Baseline_electrodes_1(:,k) = baseline_data( (2*k)-1 : interval : end, 5);
    Baseline_electrodes_2(:,k) = baseline_data( (2*k)-1 : interval : end, 7);
end
```

```matlab
electrodes_time = 0 : 1/electrodes_sampling_freq : ...
                (length(electrodes_1(:,1))-1)/electrodes_sampling_freq;

% Transform to resistance (kOhms) using BioTac equation
for k = 1:19

   Baseline_electrodes_1(:,k)=(40950-10*Baseline_electrodes_1(:,k))./Baseline_electrodes_1(:,k);
   Baseline_electrodes_2(:,k)=(40950-10*Baseline_electrodes_2(:,k))./Baseline_electrodes_2(:,k);

   electrodes_1(:,k)=(40950-10*electrodes_1(:,k))./electrodes_1(:,k);
   electrodes_2(:,k)=(40950-10*electrodes_2(:,k))./electrodes_2(:,k);
end

for k = 1:19
   electrodes_1(:,k) = electrodes_1(:,k) - Baseline_electrodes_1(300,k);
   electrodes_2(:,k) = electrodes_2(:,k) - Baseline_electrodes_2(300,k);
end

%% DC Pressure

% retrieving the electrodes' data
Pdc_sampling_freq = 100;
interval = 44;

% signals from the different BioTacs
Pdc_1 = data( 39 : interval : end, 5);
Pdc_2 = data( 39 : interval : end, 7);

Baseline_Pdc_1 = baseline_data( 39 : interval : end, 5);
Baseline_Pdc_2 = baseline_data( 39 : interval : end, 7);

Pdc_time = 0 : 1/Pdc_sampling_freq : ...
                (length(Pdc_1)-1)/Pdc_sampling_freq;

% Transform to DC pressure to psi
% x_offset is signal at rest, use mean of values from 2-3s
x_offset1 = mean(Baseline_Pdc_1);
x_offset2 = mean(Baseline_Pdc_2);

Pdc_1 = (Pdc_1-x_offset1).*0.005372;
Pdc_2 = (Pdc_2-x_offset2).*0.005372;
```